



This is a repository copy of *The chronology of Late Pleistocene thermal contraction cracking derived from sand wedge OSL dating in central and southern France*.

White Rose Research Online URL for this paper:  
<http://eprints.whiterose.ac.uk/129214/>

Version: Accepted Version

---

**Article:**

Andrieux, E., Bateman, M.D. [orcid.org/0000-0003-1756-6046](https://orcid.org/0000-0003-1756-6046) and Bertran, P. (2018) The chronology of Late Pleistocene thermal contraction cracking derived from sand wedge OSL dating in central and southern France. *Global and Planetary Change*, 162. pp. 84-100. ISSN 0921-8181

<https://doi.org/10.1016/j.gloplacha.2018.01.012>

---

**Reuse**

This article is distributed under the terms of the Creative Commons Attribution-NonCommercial-NoDerivs (CC BY-NC-ND) licence. This licence only allows you to download this work and share it with others as long as you credit the authors, but you can't change the article in any way or use it commercially. More information and the full terms of the licence here: <https://creativecommons.org/licenses/>

**Takedown**

If you consider content in White Rose Research Online to be in breach of UK law, please notify us by emailing [eprints@whiterose.ac.uk](mailto:eprints@whiterose.ac.uk) including the URL of the record and the reason for the withdrawal request.



[eprints@whiterose.ac.uk](mailto:eprints@whiterose.ac.uk)  
<https://eprints.whiterose.ac.uk/>

# 1 The chronology of Late Pleistocene thermal contraction cracking 2 derived from sand wedge dating in central and southern France

3 Eric Andrieux<sup>1</sup>, Mark D. Bateman<sup>2</sup>, Pascal Bertran<sup>1,3</sup>

4 <sup>1</sup> PACEA, UMR 5199 Université de Bordeaux – CNRS, Bâtiment B18, Allée Geoffroy-Saint-Hilaire, CS  
5 50023, 33615 Pessac cedex, France. *Email*: andrieux.e@gmail.com

6 <sup>2</sup> Department of Geography, University of Sheffield, Winter Street, Sheffield S10 2TN, UK. *Email*:  
7 m.d.bateman@sheffield.ac.uk

8 <sup>3</sup> INRAP, 140 avenue du Maréchal Leclerc, 33130 Bègles, France. *Email*: pascal.bertran@inrap.fr

9

## 10 Abstract

11 Much of France remained unglaciated during the Late Quaternary and was subjected to repeated  
12 phases of periglacial activity. Numerous periglacial features have been reported but disentangling the  
13 environmental and climatic conditions they formed under, the timing and extent of permafrost and  
14 the role of seasonal frost has remained elusive. The primary sandy infillings of relict sand-wedges and  
15 composite-wedge pseudomorphs record periglacial activity. As they contain well-bleached quartz-  
16 rich aeolian material they are suitable for optically stimulated luminescence dating (OSL). This study  
17 aims to reconstruct when wedge activity took place in two regions of France; Northern Aquitaine and  
18 in the Loire valley. Results from single-grain OSL measurements identify multiple phases of activity  
19 within sand wedges which suggest that wedge activity in France occurred at least 11 times over the  
20 last 100 ka. The most widespread events of thermal contraction cracking occurred between ca. 30  
21 and 24 ka (Last Permafrost Maximum) which are concomitant with periods of high sand availability  
22 (MIS 2). Although most phases of sand-wedge growth correlate well with known Pleistocene cold  
23 periods, the identification of wedge activity during late MIS 5 and the Younger Dryas strongly  
24 suggests that these features do not only indicate permafrost but also deep seasonal ground freezing  
25 in the context of low winter insolation. These data also suggest that the overall young ages yielded by  
26 North-European sand-wedges likely result from poor record of periglacial periods concomitant with  
27 low sand availability and/or age averaging inherent with standard luminescence methods.

28

29 **Keywords:** OSL; Luminescence dating; Sand wedge; Thermal contraction cracking; France

30

## 31 1. Introduction

32 Globally during the last glacial periglaciation extended from high to mid-latitude areas driven by  
33 overall climatic coolings. Areas beyond the ice limits experienced multiple periglacial phases and  
34 have records of these events preserved in the surficial sediments and landforms (Isarin et al., 1998;  
35 Andrieux et al., 2016a). A long-standing challenge has been to establish the relationship between  
36 preserved structures and periglacial processes and climate (e.g. Williams, 1968; Péwé, 1966;  
37 Vandenberghe, 1983; Kasse and Vandenberghe, 1998; Murton et al., 2000; Murton, 2013). This has  
38 led to attempt to model the style and extent of periglaciation in mid latitudes (e.g. Tricart, 1956;  
39 Maarleveld, 1976; Huijzer and Vandenberghe, 1998; Van Vliet-Lanoë and Hallégouët, 2001;  
40 Vandenberghe et al., 2004; 2014). A second challenge has been to understand the timing and extent  
41 of these relict periglacial features to enable linkages with other palaeoclimatic proxy records and to  
42 better understand spatial regional differences. Previous works (e.g. Buylaert et al., 2009) have  
43 undertaken this at the region scale but such studies are hampered by the often polycyclic nature of  
44 periglacial features.

45 The age of when ice and sand wedges formed remains uncertain so far in France and available data  
46 are often marred by large uncertainties. The secondary nature of the infilling of ice wedge  
47 pseudomorphs does not allow direct dating, and age estimates generally rely on bracketing dates  
48 obtained from host and cover sediments. Primary infillings in sand wedges are composed of quartz-  
49 rich aeolian material, which is suitable for optically stimulated luminescence (OSL) dating. Sand  
50 wedges are, however, far from being readily datable features. Standard OSL methods applied to a  
51 sample of sandy infilling, i.e. a cylinder 5 cm in diameter and 20 cm long, make sense only if all the  
52 sand grains have a similar depositional history. Studies in modern arctic settings suggest that such an  
53 assumption is probably not true in most cases. As shown by Mackay (1993), thermal contraction  
54 cracking occurs episodically. The millimetre-thick vertical sand laminae may thus reflect successive,  
55 discrete episodes of cracking and filling, which are potentially separated by long phases of wedge  
56 inactivity.

57 Accordingly, recent studies by Bateman (2008) and Bateman et al. (2010) pointed that OSL dating of  
58 sand wedges shows sometimes palaeodose ( $De$ ) scatter that cannot be explained by other  
59 experimental parameters such as poor recycling, sensitivity changes, variable OSL components,  
60 recuperation problems, or large  $De$  uncertainties from dim grains. This scatter may be related to  
61 multiple  $De$  components as it would be the case in a multi-phase formation model for the wedges.  
62 Consequently, the ages calculated from luminescence values yielded by aliquot measurement or/and

63 Central Age Model analysis (CAM, Galbraith et al., 1999) may not necessarily represent the true ages  
64 of the features but rather averaged values. The use of high resolution single grain measurements and  
65 the extraction of the datasets with Finite Mixture Model (FMM, Galbraith and Green, 1990), which  
66 was developed to analyse statistically data comprising multiple components, allow for the calculation  
67 of more representative ages (Bateman et al., 2010, 2014; Guhl et al., 2013).

68 This present study aims to establish for the first time a chronological framework for periglacial wedge  
69 formation in France during the Late Pleistocene. Following the approach proposed by Bateman et al.  
70 (2010), single grain OSL measurements and FMM analysis were applied to a comprehensive suite of  
71 33 samples taken from the infillings of French sand-wedges and composite-wedge pseudomorphs in  
72 order to better understand the chronology of Late Pleistocene thermal contraction cracking events.  
73 The features selected are from a number of sites located within two regions, one in Northern  
74 Aquitaine which is one of the southernmost areas of sand-wedge occurrence in France (~45°N), the  
75 other in the Loire valley in a more northern region (~47°N) (Figure 1).

76

## 77 2. Background

78 Relict periglacial wedge structures and pseudomorphs created by thermal contraction cracking in  
79 areas that underwent permafrost and/or deep seasonal freezing of the ground have been widely  
80 reported in France (Fig. 1). Ice-wedge pseudomorphs characterised by a secondary infilling replacing  
81 ice have been described in alluvial deposits of the Paris basin and in loess of northern France (e.g.  
82 Michel, 1969, 1975; Sommé and Tuffreau, 1971; Lautridou, 1985; Antoine, 1988, 1990; Lécalle, 1989;  
83 Deschodt et al., 1998; Sellier and Coutard, 2007; Feray, 2009; Moine et al., 2011; Andrieux et al.,  
84 2016a,b). These features are only found north of 47°N, and demonstrate that part of the territory  
85 was affected by permafrost during the coldest periods of the Pleistocene (Andrieux et al., 2016a).  
86 Relict epigenetic sand wedges have been discovered between 47 and 43.5°N in the vicinity of  
87 coversands in the Loire valley, Northern Aquitaine and Provence (Bouteyre and Allemann, 1964;  
88 Arnal, 1971; Antoine et al., 2005; Lenoble et al., 2012; Bertran et al., 2014; Andrieux et al., 2016a,b).  
89 Unlike ice-wedge pseudomorphs, they show a laminated or massive primary infilling of aeolian sand.  
90 Composite wedge pseudomorphs that have both primary and secondary infilling have also been  
91 described (Antoine et al., 2005; Andrieux et al., 2016a,b) but difficulties in identifying secondary  
92 infillings in sandy sedimentary contexts may have led to the classification of a large number of these  
93 features as 'sand wedges' (Andrieux et al., 2016b).

94 In Europe, North America and Asia, thermoluminescence (TL), infrared-stimulated luminescence  
95 (IRSL) and optically-stimulated luminescence (OSL) have been already applied for dating sand wedges  
96 on K-feldspars, polymineral fine grains or quartz, using multiple aliquots or single aliquots  
97 approaches. Although different techniques were used that does not ensure data homogeneity, the  
98 calculated ages provide a first chronological framework for sand wedge development during the Late  
99 Pleistocene. The largest set of OSL ages has been obtained by Buylaert et al. (2009) from 14 sand and  
100 composite-wedge pseudomorphs in Flanders, Belgium. The results suggest that most wedges (i.e. 12  
101 out of 14) were active between  $21.8 \pm 1.2$  and  $13.9 \pm 1.0$  ka. This is in agreement with the previously  
102 published ages for northern Europe (Böse, 1992, 2000; Briant et al., 2005; Kjaer et al., 2006; Kasse et  
103 al., 2007), which show that the features mostly formed during MIS 2 and the Lateglacial. Few ages fall  
104 within MIS 3 (Kolstrup and Mejdhal, 1986; Kolstrup, 2007; Christiansen, 1998). More to the south  
105 ( $47.64^\circ\text{N}$ ), two sand wedges also yielded late MIS 2 ages in Hungary (Kovács et al., 2007; Fàbiàn et al.,  
106 2014). The published OSL ages for French sand wedges (ca.  $45^\circ\text{N}$ ) are on average older and cluster  
107 between 37 and 23 ka (Guhl et al., 2013; Lenoble et al., 2012; Bertran et al., 2014). Although being  
108 part of the same polygonal network visible in aerial photographs, all the investigated wedges yielded  
109 different ages which cannot be explained by luminescence dating uncertainties. This strongly  
110 suggested that sand wedge growth was asynchronous and controlled by local conditions rather than  
111 global.

112

113 A number of cross-sections in loess from northern France, Belgium and Germany show networks of  
114 ice-wedge pseudomorphs which open generally in iron-depleted and cryoturbated horizons referred  
115 to as “tundra gleys” (i.e. Haplic Cryosols according to Kadereit et al., 2013). These serve as  
116 benchmark levels for the correlation between sections at a regional scale in northern France (Antoine  
117 and Locht, 2015). The few reliable numerical ages in direct association with the pseudomorphs  
118 highlight six events of permafrost development. The main phase is characterized by two levels of  
119 large ice wedge pseudomorphs, sometimes superimposed, and dated to ca. 25 and 30 ka respectively  
120 (Frechen et al., 2001; Locht et al., 2006; Kreutzer et al., 2012; Meszner et al., 2013; Antoine et al.,  
121 2015). This period stretches over Greenland Stadials (GS) 3, 4 and 5 (Rasmussen et al., 2014) and can  
122 be interpreted as the Last Permafrost Maximum (LPM, Vandenberghe et al., 2014). Three other levels  
123 of ice-wedge pseudomorphs associated with tundra gleys have been identified in France at  
124 Havrincourt (northern France, Antoine et al., 2014): (1) small pseudomorphs at the top of the  
125 sequence, which remain undated but are stratigraphically younger than the LPM, (2) pseudomorphs  
126 in between two soil complexes dated respectively to  $42.1 \pm 2.8$  and  $51.5 \pm 3.2$  ka, and (3) small  
127 pseudomorphs bracketed between  $61.7 \pm 4$  and  $65 \pm 3.8$  ka.

128 These ages depict a complex formation history and differ from those published for sand wedges in  
129 Northern Europe, which are unexpectedly much younger.

130

### 131 3. Study sites

132 The precise location of the studied features, the sample name and the lab codes are given in table 1.  
133 The sites of Salaunes (Château Montgaillard), Cussac-Fort-Médoc (Parcelle Lagrange), Mérignac  
134 (Chronopost) and Saint-André-de-Cubzac (ZAC Parc d'Aquitaine) are situated on the plateaus  
135 surrounding the Garonne valley (Salaunes, Saint-André-de-Cubzac) or on old alluvial terraces (Cussac-  
136 Fort-Médoc, Mérignac). The Eocene to Lower Pleistocene host sediment ranges from clayey sand to  
137 sandy gravel. All the studied wedges are epigenetic features filled with aeolian sand near the margin  
138 of Pleistocene coversands. The wedges open at the top of alluvial deposits usually capped by  
139 ventifacts. They are V-shaped, 1 to 2 m in depth, 0.3 to 0.6 m in width (measured orthogonally to the  
140 axial plane of the wedge), and have either a massive or a laminated sandy infilling (Figure 2). In total,  
141 17 samples were gathered from 5 sand wedges in these sites.

142 In the Loire valley 16 samples were taken from 6 epigenetic sand wedges (Olivet, La Flèche, La-  
143 Chapelle-aux-Choux, Challans) and 2 composite wedge pseudomorphs (Durtal, Sainte-Geneviève-des-  
144 Bois) (table 1, Figure 2). The wedges develop within Pleistocene alluvial terraces composed of sandy  
145 gravel, in close proximity of rivers which provided abundant aeolian sand during the glacials. The  
146 wedges are 0.3 to 1 m wide and 1 to 2.5 m in depth. At Durtal a primary laminated sandy infill (0.3 m  
147 wide, 1.7 m depth) cross-cuts a previous secondary infill composed of massive sandy gravel (1 m  
148 wide, 2 m in depth). The composite-wedge pseudomorph at Sainte-Geneviève-des-Bois, 1.2 m wide  
149 and 1.7 m in depth, shows a primary massive sandy infill cross-cut by a secondary silty infill which  
150 exhibits U-shaped lamination. The site of Saint-Christophe-du-Ligneron (Challans) is located south of  
151 the Loire estuary in the vicinity of a small coversand area.

152

### 153 4. Methodology

#### 154 4.1 Sample collection and preparation

155 Thirty-three samples were collected for OSL from the sandy infillings of freshly exposed sand wedges  
156 or composite wedge pseudomorphs by hammering in the sections opaque PVC tubes or metal tubes  
157 (60 mm in diameter, 250 mm long). To get a better chance of recording different events potentially  
158 preserved in the wedges multiple samples were taken along a horizontal line in the infilling of each

159 wedge when possible. Vertical samples were taken within the primary infillings to check for the  
160 influence of depth on doses. The host sediments were also sampled for gamma dose rate modelling  
161 purposes.

162 The samples were prepared under subdued red light conditions at the Sheffield Luminescence  
163 Laboratory. To avoid any potential light contamination that may have occurred during sampling, 2 cm  
164 of sediment located at the ends of the PVC tubes was removed and used for estimations of  
165 palaeomoistures. The light-unexposed material was treated with hydrochloric acid (1M, HCl) and  
166 hydrogen peroxide (H<sub>2</sub>O<sub>2</sub>) to remove carbonates and organic matter. To ensure that only one grain  
167 will fit into each hole when mounted on discs for single grain analysis and to minimise intra-sample  
168 variability dry sieving of the sediment was performed, and the 180-250 µm fraction size was kept for  
169 OSL measurement. Heavy liquid treatment with sodium polytungstate at 2.67 g.cm<sup>-3</sup> allowed the  
170 separation of quartz from sediment of higher specific gravity (i.e. heavy minerals). The remaining  
171 sediment was then treated with hydrofluoric acid (HF) to etch the grain surface and to remove  
172 residual feldspars and light minerals other than quartz. Once dry, the sediment was treated again  
173 with HCl, and then re-sieved at 180 µm to remove acid-soluble fluorides and any grains that have  
174 been significantly reduced in size by etching.

175

#### 176 4.2 Dose rate determination

177 Dose rates to individual samples are based on elemental measurements made using inductively-  
178 coupled plasma mass spectrometry (ICP-MS) as in situ gamma-spectrometer were not possible. This  
179 was carried out at the laboratories of SGS Canada ([www.sgs.ca](http://www.sgs.ca)). Insofar as most wedges are less than  
180 0.5 m in width, it was generally not possible to sample 0.3 m away from the host sediment, which is  
181 the maximum travelled distance by gamma rays. Therefore, the adjacent different lithostratigraphic  
182 units of host sediment were also measured to establish their contribution to the gamma dose rate.  
183 Gamma dose rates were modelled and corrected using the scaling factors of Aitken (1985) and had  
184 little impact on the total doses. Elemental concentrations were converted to annual dose rates using  
185 data from Guérin et al. (2011). In order to adjust the dose rates, the following attenuation factors  
186 were used: (i) alpha and beta grain size attenuation effects from Bell (1980), Mejdhal (1979) and  
187 Readhead (2002), (ii) an a-value of  $0.10 \pm 0.02$  for coarse grain quartz (Olley et al. 1998), (iii) an etch  
188 attenuation factor after Duller (1992), and (iv) an attenuation for palaeomoisture content based on  
189 moisture content at time of sampling with an absolute error of  $\pm 5\%$  incorporated to allow for past  
190 changes. The contribution to dose rates from cosmic sources is a function of geographic location,  
191 burial depth and altitude and was calculated using the algorithms published in Prescott and Hutton

192 (1994). An internal quartz dose rate of 10  $\mu\text{Gy}/\text{ka}$  was added to the total dose rate as done by  
193 Vandenberghe et al. (2008). The dosimetry results are available in table 2.

194

#### 195 4.3 Luminescence measurements

196 Luminescence measurements were performed on a Risø reader TL-DA-15 equipped with a  $^{90}\text{Sr}/^{90}\text{Y}$   
197 beta source for irradiation (Bøtter-Jensen et al., 2003). The reader was fitted with a single grain  
198 attachment that used a 10 mW Nd:YVO<sub>4</sub> solid state diode-pumped laser emitting at 532 nm, which  
199 produced a spot approximately 50  $\mu\text{m}$  in diameter (Duller et al., 1999), allowing simulation of  
200 individual grains. The luminescence emissions were detected through a Hoya U-340 filter. The purity  
201 of extracted quartz was tested for each sample by stimulation with infra-red light as per Duller  
202 (2003). No samples showed signs of feldspar contamination. Single grains were measured on 9.6 mm  
203 diameter aluminium discs containing 100 holes.

204

205 Equivalent dose ( $D_e$ ) determination was carried out using the Single-Aliquot Regenerative-dose (SAR;  
206 Murray and Wintle, 2000, 2003; Table A1). A four point SAR protocol was employed to bracket the  
207 expected palaeodoses with an additional recycling point to check for uncorrected sensitivity  
208 changes (Figure A1). Preheat temperatures were determined using a dose recovery preheat plateau  
209 test (Murray and Wintle, 2003). The samples displayed OSL decay curves dominated by the fast  
210 (bleachable) component, had good dose recovery, low thermal transfer and good recycling (Figure  
211 A2).  $D_e$  values were only accepted when the recycling ratio was comprised between 0.8 and 1.2,  
212 recuperation on zero dose was lower than 5%, and the error on the  $D_e$  was less than 30%. The grains  
213 exhibiting a signal that was not possible to fit by an exponential, or exponential plus linear growth  
214 curve were rejected. However, when the palaeodose could not be ascertained for a grain due to  
215 saturation it was recorded as it gives important information on the sample. A minimum of 50  $D_e$   
216 values which met the quality acceptance criteria were measured for each sample to ensure a  
217 representative spread in  $D_e$  values and to assess the degree of scatter and skewness of the data. Only  
218 2 to 4% of the grains had a measurable OSL signal that met the selection criteria. The samples  
219 CAH2.1, CAH2.2, CAH2.3, CAH4.1 and CAH4.2 from the Loire valley had between 10 to 20% saturated  
220 grains, whereas the samples from Northern Aquitaine do not show any saturation. Potential  
221 contamination by host material was checked during sampling and preparation. No evidence for  
222 mixing of different material was found.



223 The measurements of the OSL signal at single grain level show a large  $D_e$  heterogeneity with high  
224 overdispersion (Figure 3; Figure A3). As for the sand wedge investigated by Bateman et al. (2008,  
225 2010) the scatter of the  $D_e$  values cannot be explained by poor recycling, recuperation problems, or  
226 sensitivity changes. In few sampled wedges sand lamination was visible, which testifies to the lack of  
227 post-depositional perturbation of the primary infilling. However, a significant amount of the samples  
228 were taken from massive sand bodies or from infillings where lamination was only locally preserved,  
229 which probably indicate that subsequent mixing occurred due to ice thaw, bioturbation and other  
230 pedoturbations (Murton et al., 2000). Such processes may have lead to the inclusion of partially  
231 bleached grains in the wedges coming from the surrounding ground surface or from the host  
232 sediment, which can result in long tails of  $D_e$  or in broad distributions rather than in discrete peaks.  
233 The scatter of data is thus assumed to be caused either by poor bleaching of grains prior burial or by  
234 the mixing of different age deposits.

235 An averaging issue would arise if the Central Age model (CAM; Galbraith et al 1999, Roberts et al.,  
236 2000) was used to extract the  $D_e$  values since this model is designed for well-bleached samples. The  
237 standard approaches are to use either the Minimum Age Model (MAM; Galbraith and Laslett, 1993)  
238 or the Finite Mixture Model (FMM; Galbraith and Green 1990) to calculate age estimates. FMM  
239 allows the extraction of  $D_e$  components within  $D_e$  distributions and MAM extract the component  
240 that provide the minimum age. In our case this means that FMM date the different periods of  
241 periglacial wedge infilling while MAM gives the estimate of the last time the wedge was active. Both  
242 models were used to calculate the age estimates of the wedges. However, FMM was considered  
243 more appropriate because of the potential multi-phased nature of sand-wedges. As the CAM is the  
244 model used in previous dating of sand-wedges, the CAM ages were calculated for comparison  
245 purposes.

246

247 For FMM a  $\sigma_b$  value of 0.15 was chosen based on dose recovery tests. The best fit was assessed by  
248 iteratively increasing the number ( $k$ ) of components until the closest to zero value of the Bayesian  
249 Information Criterion (BIC) was reached. To avoid the influence of potential post-contamination the  
250  $D_e$  components were considered only when exceeding 10% of the total  $D_e$  values for each sample  
251 (Bateman et al., 2007).

252

253 5. Results

254 FMM analysis allowed extraction of two to four components for each of the 33 samples from which a  
255 total of 86 age estimates were calculated, 47 in the Loire valley and 39 in Northern Aquitaine  
256 respectively (table 3). The OSL ages range between  $337 \pm 40$  ka and  $7.5 \pm 1.2$  ka.

257 In order to test the assumption that wedge activity was not random during the last glacial but rather  
258 occurred during specific, climate-controlled periods, the cumulated probability density of the ages  
259 was calculated using Oxcal 4.2 (Bronk Ramsey, 2013) with the expectation that peaks would emerge  
260 from the probability distribution. As this was the case, the distribution was adjusted to a combination  
261 of Gaussian functions using the software Fityk 0.9.8 (Wojdyr, 2010) and their respective contribution  
262 was calculated. The goodness of fit was assessed using  $R^2$ , which reached almost unity ( $R^2=0.9999$ ).  
263 The standard deviation of the distribution around the centre of each Gaussian function was  
264 estimated from the Full Width at Half Maximum (FWHM). The PDF was plotted together with the  
265 NGRIP  $\delta O^{18}$  data over the last 100 ka tuned to the revised Greenland Ice Core Chronology proposed  
266 by Rasmussen et al. (2014) to compare the thermal contraction cracking events with known cooling  
267 occurrences over Europe (Figure 4). The results suggest the following:

- 268 i) The sand wedges and composite wedge pseudomorphs were repeatedly active during the Middle  
269 and Late Pleistocene up to the beginning of the Holocene.
- 270 ii) The oldest events are recorded in the Loire valley where 71% of OSL ages fall within MIS 3, 4 and  
271 5. In contrast, MIS 2 represent up to 54% of the total OSL ages in Northern Aquitaine. In the latter  
272 area, the oldest age falls within MIS 4.
- 273 iii) A total of 11 peaks of wedge activity have been extracted from the 86 ages provided by the  
274 samples from the whole dataset during the last 100 ka, i.e.  $8.5 \pm 0.6$ ,  $11.9 \pm 0.5$ ,  $15.3 \pm 0.4$ ,  $17.4 \pm$   
275  $0.7$ ,  $20.7 \pm 0.7$ ,  $24 \pm 1.1$ ,  $30 \pm 2.5$ ,  $42.5 \pm 1.9$ ,  $56.2 \pm 4$ ,  $71.4 \pm 1.8$ ,  $86 \pm 4.2$  ka
- 276 iv) Seven OSL ages are older than 100 ka and may correspond to cracking events that occurred  
277 during MIS 6, 8 or 10.

278 The PDFs of the estimates calculated with the different age models (i.e. CAM, MAM, and FMM) allow  
279 for comparisons (Figure 5). Differences between the models are evident. As expected the CAM based  
280 dataset by averaging all grains from samples identifies fewer more prominent phases of wedge  
281 activity during MIS 2. The MAM based dataset by selecting only the youngest component of grains  
282 from a sample, under-estimates the earlier phases of wedging. The FMM datasets by attempting to  
283 isolate similar age components within samples provides a longer record with more phases within it.

284 As shown on a representative case study in figure 6, the calculated ages are much younger than the  
285 host material of the wedges. They overlap from one sample to another within the same wedge, and  
286 between different wedges, and they are not dependent on depth.

287

## 288 6. Discussion

## 289 6.1. France

290 The overall age distribution of periglacial wedges shows repetitive thermal contraction cracking over  
291 the last 100 ka. However, substantial differences emerge from the comparison between the two  
292 regions. Two main factors may be involved, which include:

293 (1) The latitude of the investigated wedges. As expected, the Loire valley yields a larger number of  
294 ages falling into MIS 5 to 3 than does Northern Aquitaine which is located at lower latitude. Overall,  
295 the first area is assumed to have been more frequently affected by deep seasonal freezing and/or  
296 permafrost during the Late Pleistocene.

297 (2) The sand availability. In addition to the temperature drop that triggers thermal contraction  
298 cracking, the main limiting factor in the growth of sand-wedges is the sand supply. In the Loire valley  
299 the sand has a fluvial origin, and sand drifting was probably active during the stadials all along the  
300 last glacial on bare alluvial deposits exposed to deflation. In contrast, the location of the sand wedges  
301 of Northern Aquitaine near the margin of the coversands ("Sables des Landes" Formation, Sitzia et  
302 al., 2015) strongly suggests that this formation, which was fed by deflation on the continental plateau  
303 exposed during sea-level lowstands, was the main sand source that filled the contraction cracks.  
304 Available chronological data (Bertran et al., 2011; Sitzia et al., 2015) show that the coversands built  
305 up mostly between ca. 24 and 14 ka. Comparison between the distribution of ages for coversands  
306 and sand wedges points to strong similarity, suggesting that the latter primarily record periods where  
307 thermal contraction cracking and huge sand drifting in the coversand area occurred at once (Figure  
308 7). To a certain extent, this record may, therefore, be biased toward MIS 2 which corresponds to the  
309 main phase of coversand emplacement.

310 Age clusters were identified in both areas within the Lateglacial (12 ka, i.e. Younger Dryas, 5 dates in  
311 whole data set) and, more surprisingly, within the early Holocene at 8.5 ka (5 dates). Since the De  
312 components of the early Holocene are only slightly above the 10% chosen threshold, it cannot be  
313 excluded that these ages reflect sample contamination due to localised bioturbation. Wedge activity  
314 during the Younger Dryas, which were typified by mean annual air temperatures too high for  
315 permafrost development in France (Renssen and Isarin, 1998; Simonis et al., 2012), reinforces the  
316 assumption that these features are poor indicators of past permafrost as already suggested by  
317 Andrieux et al. (2016a) and Wolfe et al. (2016). Younger Dryas mean January air temperature are  
318 poorly constrained by available biological records, however, beetle proxies (Ponel et al., 2007) point

319 to rather cold winters (min January temperatures estimated between -3 to -18°C), probably because  
320 of low winter insolation (Berger, 1978). This allowed deep seasonal ground freezing to occur. Sand  
321 drifting was still active in European coversand areas during the Younger Dryas (Kasse, 2002; Sitzia et  
322 al., 2015). In Aquitaine, fields of parabolic dunes developed on large areas at that time (Bertran et al.,  
323 2011). More recent sand wedge activity was unexpected, since temperatures rose significantly in the  
324 early Holocene, although the seasonal contrast remained high compared to present. Considering the  
325 uncertainty associated with the OSL ages and assuming that these ages do not reflect contamination,  
326 we suggest here that the recorded thermal contraction events reflect the impact of the short cooling  
327 events identified at 9.3 and 8.2 ka in the Greenland ice cores (Rasmussen et al., 2014) and in other  
328 proxy records (Wanner et al., 2011). They would also indicate that sand was still mobile at least  
329 locally and not yet totally fixed by vegetation.

330 MIS 2 is a period characterized by strong wedge activity, and includes up to 54% of the ages (i.e. 21  
331 dates) of the Northern Aquitaine data set (phases 3 to 6, Fig. 4). Both regions record wedging at the  
332 beginning and in the middle of Greenland Stadial 2 (GS 2.1) around respectively 17.5 ka (GS 2.1a) and  
333 21 ka (GS 2.1c), and around 24 ka at the end of GS 3. Another cluster is identified at 15.5 ka (late  
334 GS 2.1) only in Northern Aquitaine. The absence of record of this contraction cracking phase in the  
335 Loire valley may be explained as follows:

336 (1) Sand availability and/or deflation were limited in regions distant from the main coversand areas.  
337 However, the reason why this occurred specifically during this period remains hard to explain.

338 (2) The higher number of ages obtained in Northern Aquitaine allows better precision in the  
339 calculation of peaks, which are typified by low FWHM. This highlights the sensitivity of the method  
340 used for identifying the major phases of wedge growth to the size of the data set. Further dating will  
341 make it possible to improve the representativeness of the identified phases.

342 A period of widespread thermal contraction cracking which is common to both study areas is also  
343 recorded during the end of MIS 3 at approximately 30 ka (GS 5) (phase 7, Fig. 4). Older wedge activity  
344 is mostly detected in the Loire valley. Clustering of ages appears less obvious, however, and the  
345 identified phases have to be considered with caution. The most preeminent phase took place at ~56  
346 ka, i.e. probably at the very end of MIS 4 taking into account the luminescence dating uncertainties  
347 (phase 9, Fig. 4). It is worth noting that a significant number of ages (6 dates) fall within late MIS 5  
348 which was typified on average by a mild climate. PDF analysis suggests that they cluster around ~86  
349 ka, i.e. during the stadial GS 22 (phase 11, Fig. 4) . As for the early Holocene, this period coincides  
350 with a minimum in winter insolation (Berger, 1978).

351 Although it is not possible to define  $D_e$  values for saturated grains, their presence within the  
352 investigated wedges is interpreted as reflecting phases of thermal contraction cracking that are  
353 beyond the limit of the luminescence dating method on quartz. The saturated grains come from  
354 samples that provided the oldest ages, i.e. MIS 8 or 10.

355 In some wedges (Salaunes, Mérignac and Cussac-Fort-Médoc) the samples taken from the sides of  
356 the infilling have yielded older ages than those from the middle. This has to be interpreted as the  
357 preferred preservation of early phases of activity in the sides of the wedges.

358

## 359 6.2. Comparison with the records of Northern Europe

360 The analysis presented here show that the thermal contraction events previously identified in the  
361 loess deposits of northern France were also recorded in the sand wedges and composite wedge  
362 pseudomorphs from southwest France and the Loire valley. Particularly, the two main levels of large  
363 ice-wedge pseudomorphs dated to 30 and 25 ka (Antoine et al., 2014; Bertran et al., 2014) in the  
364 loess sequences have their counterparts in sand wedges (ca. 30 and 24 ka respectively). Such a  
365 synchronicity testifies to widespread events of thermal contraction cracking in France, which are  
366 thought to coincide with the last maximum of permafrost extension. In the marine realm, these  
367 events correspond to Heinrich Stadials 3 and 2 respectively (Sanchez-Goñi and Harrison, 2010).  
368 Because of the scarcity of available ages, more in detail fitting of the records remains impossible both  
369 for older and younger phases. Overall, the number of the phases of wedge development appears to  
370 be larger in the sand wedges than in loess. The following factors may be involved:

371 (1) Poor preservation of ice-wedge pseudomorphs due to thermokarst processes (Locht et al., 2006).  
372 Strong pedoturbation at the top of loess sequences during the Holocene may also have obscured or  
373 made illegible MIS 2 features.

374 (2) Lack of permafrost and associated growth of large ice bodies susceptible to produce  
375 pseudomorphs. Thermal contraction cracking in the context of deep seasonal freezing of the ground  
376 created sand wedges where sand drifting was active, but only tiny fissures elsewhere. This was  
377 especially the case for Late MIS 5 and the Lateglacial.

378 Using a same approach to that used here on periglacial patterned ground (polygons and stripes)  
379 found in East Anglia, UK, Bateman et al. (2014) found similar phases of activity during the last 90 ka at  
380 55–60 ka (MIS 4), 31–35 ka (MIS 3), 20–22 ka (GS2.1c) and 11–12 ka (GS1). However, most of the  
381 previous age estimates for sand wedges from northern Europe fall within late MIS 2 and the

382 Lateglacial, i.e. during the main periods of coversand emplacement. In contrast to loess sequences,  
383 almost no wedge activity is recorded within late MIS 3 and early MIS 2. In the light of our data, this  
384 pattern has to be interpreted as reflecting two main factors: (1) limited record of thermal contraction  
385 phases during periods with low sand availability, (2) the use of aliquot and/or CAM analysis for the  
386 calculation of age estimates, which led to averaging the signal. This skewed the ages in favour of the  
387 most prominent phases of activity and hampered identification of the multiple events of sand wedge  
388 growth. Although a few studies in North America have suggested that distinct generations of sand  
389 wedges or multi-phased wedges occurred (French et al., 2003; Bateman et al., 2010), multiple-dose  
390 populations within wedges in Europe (Kolstrup, 2004) or unexpected ages were often attributed to  
391 partial bleaching of the sand grains due to sediment mixing and were thus rejected.

392

## 393 7. Conclusion

394 The application of single grain OSL to 33 samples taken from sand and composite wedges in France  
395 allowed identifying of multi-phased thermal contraction events within single preserved wedge  
396 features. FMM analysis identified two to four components for each sample and resulted in the  
397 calculation of 86 age estimates, each corresponding to a period of ground cracking. These show that  
398 wedges were active during Late Pleistocene cooling periods when thermal contraction and sand  
399 drifting in the coversand areas occurred at the same time, i.e. dominantly during MIS 2. Synchronicity  
400 between the ages provided by ice-wedge pseudomorphs, sand-wedges and composite-wedges in  
401 France testifies to widespread events of thermal contraction cracking between ca. 30 and 24 ka (Last  
402 Permafrost Maximum). Late MIS 5 and Early Holocene events also suggest that wedging occurred in  
403 connection with deep seasonal ground freezing during phases with marked seasonality. In  
404 comparison, the mainly late MIS2 – Younger Dryas ages yielded by North-European sand wedges are  
405 interpreted as reflecting poor record of the periods with low sand supply. In addition, the potential  
406 averaging issue inherent with the use of aliquots and CAM analysis for the dating of sand-wedges  
407 may have biased the ages towards the major phases of activity and have hampered the identification  
408 of multiple periods of opening.

409 By providing the first chronological framework for thermal contraction cracking in France, this study  
410 shows that sand-wedges and composite-wedge pseudomorphs are significant, but complex archives  
411 of the Pleistocene periglacial environments. Our results allow reassessing the periglaciation of France  
412 and its timing across Western Europe. However, owing to OSL uncertainties more effort in dating is  
413 required to improve the accuracy of the identified phases of thermal contraction cracking. The

414 multiplication of study areas in Europe should also make it possible to highlight the latitudinal  
415 fluctuations of periglacial processes during the last glacial.

416

#### 417 Acknowledgements

418 This work benefitted from funds provided by the Institut National de Recherches Archéologiques  
419 Préventives (Inrap), the Lascarbx (program of the Agence National de la Recherche ANR-10-LABX-52),  
420 the University of Bordeaux, and the PACEA laboratory. EA wishes to acknowledge the department of  
421 Geography, University of Sheffield, whilst a visiting scientist. Mark Bateman, Robert Ashurst and  
422 Alicia Medialdea are also thanked for their assistance in preparing and dating the samples.

423

#### 424 References

- 425 Aitken, M.J., 1985. Thermoluminescence dating. Academic Press, Orlando, Florida, 359 p.
- 426 Andrieux, E., Bertran, P., Saito K., 2016a. Spatial analysis of the French Pleistocene permafrost by a  
427 GIS database. *Permafrost and Periglacial Processes*, 27 (1), 17-30.
- 428 Andrieux, E., Bertran, P., Antoine, P., Deschodt, L., Lenoble, A., Coutard, S., 2016b. Database of  
429 pleistocene periglacial features in France: description of the online version », *Quaternaire*, 27/4, 329-  
430 339.
- 431 Antoine, P., 1988. Contribution à l'étude des loess du Pléistocène supérieur du bassin de la Somme.  
432 *Revue Archéologique de Picardie* 1-2, 25-44.
- 433 Antoine, P., 1990. Chronostratigraphie et environnement du Paléolithique du Bassin de la Somme.  
434 Publication du centre d'Etude et de Recherches Préhistoriques de Lille (CERP) 2, 231 pp.
- 435 Antoine, P., Marchiol, A., Brocanel, M., Gros Y., 2005. Découverte de structures périglaciaires (sand-  
436 wedges et composite-wedges) sur le site de stockage de déchets radioactifs de l'Aube (France).  
437 *Comptes Rendus Géosciences*, 337 (16), 1462-1473.
- 438 Antoine, P., Goval, E., Jamet, G., Coutard, S., Moine, O., Hérisson, D., Auguste, P., Guérin, G., Lagroix,  
439 F., Schmidt, E., Robert, V., Debenham, N., Meszner, S., Bahain, J.J., 2014. Les séquences Loessiques  
440 Pléistocène supérieur d'Havrincourt (Pas-de-Calais, France) : stratigraphie, paléoenvironnements,  
441 géochronologie et occupations paléolithiques. *Quaternaire*, 4, p. 321-368.

- 442 Antoine, P., Loch, J.L., 2015. Chronostratigraphie, paléoenvironnements et peuplements au  
443 Paléolithique moyen : les données du nord de la France. *Mémoire de la Société Préhistorique*  
444 Française , 59 , 11-23.
- 445 Antoine, P., Moncel, M.H., Loch, J.L., Limondin-Lozouet, N., Auguste, P., Stoetzel, E., Dabkowski, J.,  
446 Voinchet, P., Bahain, J.J., Falgueres, C., 2015. Dating the earliest human occupation of Western  
447 Europe: New evidence from the fluvial terrace system of the Somme basin (Northern France).  
448 *Quaternary International*, 370, 77-99.
- 449 Arnal, H., 1971. Les sols polygonaux étirés et sols striés d'âge würmien de Laudun (Gard). *Bulletin de*  
450 *l'Association Française pour l'Etude du Quaternaire*, 8 (3), 151-160.
- 451 Bailey, R.M., Arnold, L.J., 2006. Statistical modelling of single grain quartz De distributions and an  
452 assessment of procedures for estimating burial dose. *Quaternary Science Reviews*, 25, 2475-2502.
- 453 Bateman, M.D., 2008. Luminescence dating of periglacial sediments and structures: a review. *Boreas*  
454 37, 574-588.
- 455 Bateman, M.D., Boulter, C.H., Carr, A.S., Frederick, C.D., Peter, D., Wilder, M., 2007. Preserving the  
456 palaeoenvironmental record in Drylands: Bioturbation and its significance for luminescence derived  
457 chronologies. *Sediment Geology*, 195, 5-19.
- 458 Bateman, M.D., Hitchens, S., Murton, J.B., Lee, J.R., Gibbard, P.L., 2014. The evolution of periglacial  
459 patterned ground in East Anglia, UK. *Journal of Quaternary Science*, 29, 301–317.
- 460 Bateman, M.D., Murton, J.B., Boulter, C., 2010. The source of De variability in periglacial sand  
461 wedges: Depositional processes versus measurement issues. *Quaternary Geochronology*, 5, 250-256.
- 462 Bell, W.T., 1980. Alpha attenuation in Quartz grains for Thermoluminescence Dating. *Anc. TL* 12, 4-8.
- 463 Berger, A., 1978. Long-term variations of daily insolation and Quaternary climatic changes. *J. Atmos.*  
464 *Sci.*, 35(12), 2362–2367.
- 465 Bertran, P., Bateman, M., Hernandez, M., Lenoir, M., Mercier, N., Millet, D., Tastet, J.P., 2011. Inland  
466 Aeolian deposits of southwest France: facies, stratigraphy and chronology, *Journal of Quaternary*  
467 *Science*, 26, 374-388.
- 468 Bertran, P., Andrieux, E., Antoine, P., Coutard, S., Deschodt, L., Gardère, P., Hernandez, M., Legentil,  
469 C., Lenoble, A., Liard, M., Mercier, N., Moine, O., Sitzia, L., Van Vliet-Lanoë, B., 2014. Distribution and



- 470 chronology of Pleistocene permafrost features in France: database and first results. *Boreas*, 43 (3),  
471 699-711.
- 472 Böse, M., 1992: Late Pleistocene sand-wedge formation in the hinterland of the Brandenburg stade.  
473 *Sveriges Geologiska Undersökning Series Ca 81*, 59-63.
- 474 Böse, M., 2000. Gravel analysis of Weichselian tills and OSL dates of sand wedges in western Poland.  
475 *Quaestiones Geographicae* 21, 39-44.
- 476 Bøtter-Jensen, L., Andersen, C.E., Duller, G.A.T., Murray, A.S., 2003. Developments in radiation,  
477 stimulation and observation facilities in luminescence measurements. *Radiation Measurement* 37,  
478 535-541.
- 479 Bouteyre G., Allemann M., 1964. Sur quelques phénomènes périglaciaires en Costières du Gard. Un  
480 réseau polygonal de fentes en coin. *Bulletin de la Société des Sciences Naturelles de Nimes* L, 84-96.
- 481 Briant, R.M., Bateman, M.D., Russell Coope, G., Gibbard, P.L., 2005. Climatic control on Quaternary  
482 fluvial sedimentology of a Fenland Basin river, England. *Sedimentology*, 52, 1397-1423.
- 483 Bronk Ramsey, C., Lee, S., 2013. Recent and Planned Developments of the Program OxCal.  
484 *Radiocarbon*, 55(2-3), 720-730.
- 485 Buylaert, J.P., Ghysels, G., Murray, A.S., Thomsen, K.J., Vandenberghe, D., De Corte, F., Heyse, I., Van  
486 den Haute, P., 2009. Optically dating of relict sand wedges and composite-wedge pseudomorphs in  
487 Flanders, Belgium. *Boreas*, 38, 160-175.
- 488 Christiansen, H.H., 1998. Periglacial sediments in an Eemian–Weichselian succession at Emmerlev  
489 Klev, southwestern Jutland, Denmark. *Palaeogeography, Palaeoclimatology, Palaeoecology* 138, 245–  
490 258.
- 491 Deschodt, L., Djemali, N., Drwila, G., Feray, P., Teheux, E., 1998. Onnaing (59), usine Toyota. 62 pp.  
492 *Rapport des sondages archéologiques profonds*, Inrap, Amiens.
- 493 Duller, G.A.T., 1992. Luminescence Chronology of Raised Marine Terraces, South-West North Island,  
494 New Zealand. PhD thesis. University of Wales, Aberystwyth.
- 495 Duller, G.A.T., 2003. Distinguishing quartz and feldspar in single grain luminescence measurements.  
496 *Radiation Measurements* 37, 161-165.

- 497 Duller, G.A.T., Bøtter-Jensen, L., Murray, A.S., Truscott, A.J., 1999. Single grain laser luminescence  
498 (SGLL) measurements using a novel automated reader. *Nuclear Instruments and Methods in Physics*  
499 *Research B* 155, 506-514.
- 500 Fàbiàn, S.A., Kovács, J., Varga, G., Sipos, G., Horvath, Z., Thamo\_Bozso, E., Toth, G., 2014. Distribution  
501 of relict permafrost features in the Pannonian Basin, Hungary. *Boreas*, Vol. 43, pp. 722-732.
- 502 Feray, P., 2009. Feignies (59), « Les Mottes », « Queue Bizenne » et « Grand Bray » : Extension de la  
503 zone d'activité du Parc de Grévaux les Guides. 51 pp. Rapport Final d'Opération, diagnostic  
504 archéologique, Inrap, Amiens.
- 505 Frechen, M., Van Vliet-Lanoë, B., Van den Haute, P., 2001. The Upper Pleistocene loess record at  
506 Harmignies/Belgium - High resolution terrestrial archive of climate forcing. *Palaeogeography,*  
507 *Palaeoclimatology, Palaeoecology* 173, 175-195.
- 508 French, H.M., Demitroff, M., Forman, S.L., 2003. Evidence for Late-Pleistocene Permafrost in the New  
509 Jersey Pine Barrens (Latitude 39°N), Eastern USA. *Permafrost and Periglacial Processes* 14, 259-274.
- 510 Galbraith, R.F., Green, P.F., 1990. Estimating the component ages in a finite mixture. *International*  
511 *Journal of Radiation Applications and Instrumentation. Part D. Nuclear Tracks and Radiation*  
512 *Measurements* 17, 197-206.
- 513 Galbraith, R.F., Laslett, G.M., 1993. Statistical models for mixed fission track ages. *Nuclear Tracks and*  
514 *Radiation Measurements* 21, 459-470.
- 515 Galbraith, R.F., Roberts, R.G., Laslett, G.M., Yoshida, H., Olley, J.M., 1999. Optical dating of single and  
516 multiple grains of quartz from Jinmium Rock Shelter, Northern Australia: Part I, Experimental design  
517 and statistical models. *Archaeometry* 41, 339-364.
- 518 Guérin, G., Mercier, N., Adamiec, G., 2011. Dose-rate conversion factors: update. *Anc.TL*, 29, 5-8.
- 519 Guhl, A., Bertran, P., Fitzsimmons, K.E., Zielhofer, C., 2013. Optically stimulated luminescence (OSL)  
520 dating of sand-filled wedges structures and their alluvial host sediments from Jonzac, SW France.  
521 *Boreas* 42, 317-332.
- 522 Huijzer, B., Vandenberghe, J., 1998. Climatic reconstruction of the Weichselian Pleniglacial in  
523 northwestern and central Europe. *Journal of Quaternary Science*, 13(5), 391-417.

- 524 Isarin, R., Huijzer, B., van Huissteden, K., 1998. Time-slice oriented multiproxy database (MPDB) for  
525 palaeoclimatic reconstruction. National Snow and Ice Data Center, University of Boulder, Colorado.  
526 <http://nsidc.org/data/ggd248.html>
- 527 Kadereit, A., Kind, C.J., Wagner, G.A., 2013. The chronological position of the Lohne Woil in the  
528 Nussloch loess section – re-evaluation for a European loess-marker horizon. *Quaternary Science*  
529 *Reviews* 59, 67-89.
- 530 Kasse, C., 2002. Sandy aeolian deposits and environments and their relation to climate during the  
531 Last Glacial Maximum and Lateglacial in northwest and central Europe. *Progress in Physical*  
532 *Geography* 26, 4, 507-532.
- 533 Kasse, C., Vandenberghe, J., 1998. Topographic and drainage control on Weichselian ice-wedge and  
534 sand-wedge formation, Vennebrügge, German–Dutch border. *Permafrost and Periglacial Processes* 9,  
535 95–106.
- 536 Kasse, C., Vandenberghe, D., de Corte, F., van den Haute, P., 2007. Late Weichselian fluvio-aeolian  
537 sands and coversands of the type locality Grubbenvorst (southern Netherlands): sedimentary  
538 environments, climate record and age. *Journal of Quaternary Science* 22, 7, 695–708.
- 539 Kjaer, K.H., Lagerlun, E., Adrielsson, L., Thomas, P.J., Murray, A., Sandgren, P., 2006. The first  
540 independent chronology of Middle and Late Weichselian sediments from southern Sweden and the  
541 island of Bornholm. *GFF*, 128, 209-220.
- 542 Kolstrup, E., 2004. Stratigraphic and Environmental Implications of a large ice-wedge cast at  
543 Tjaereborg, Denmark. *Permafrost and Periglacial Processes*, 15, 31-40.
- 544 Kolstrup, E., 2007. OSL dating in palaeoenvironmental reconstructions. A discussion from a user's  
545 perspective. *Estonian Journal of Earth Sciences*, 56, 157-166.
- 546 Kolstrup, E., Mejdhal, V., 1986. Three frost wedge casts from Jutland (Denmark) and TL dating of their  
547 infill. *Boreas* 15, 311-321.
- 548 Kovács, J., Fàbiàn, S.A., Schweitzer, F., Varga, G., 2007. A relict sand-wedge polygon site in north-  
549 central Hungary. *Permafrost and Periglacial Processes*. 18, 379-384.
- 550 Kreutzer, S., Lauer, T., Meszner, S., Krbetschek, M.R., Faust, D., Fuchs, M., 2012. Chronology of the  
551 Quaternary profile Zeuchfeld in Saxony-Anhalt / Germany – a preliminary luminescence dating study.  
552 *Zeitschrift für Geomorphologie fast track*, 1–21.

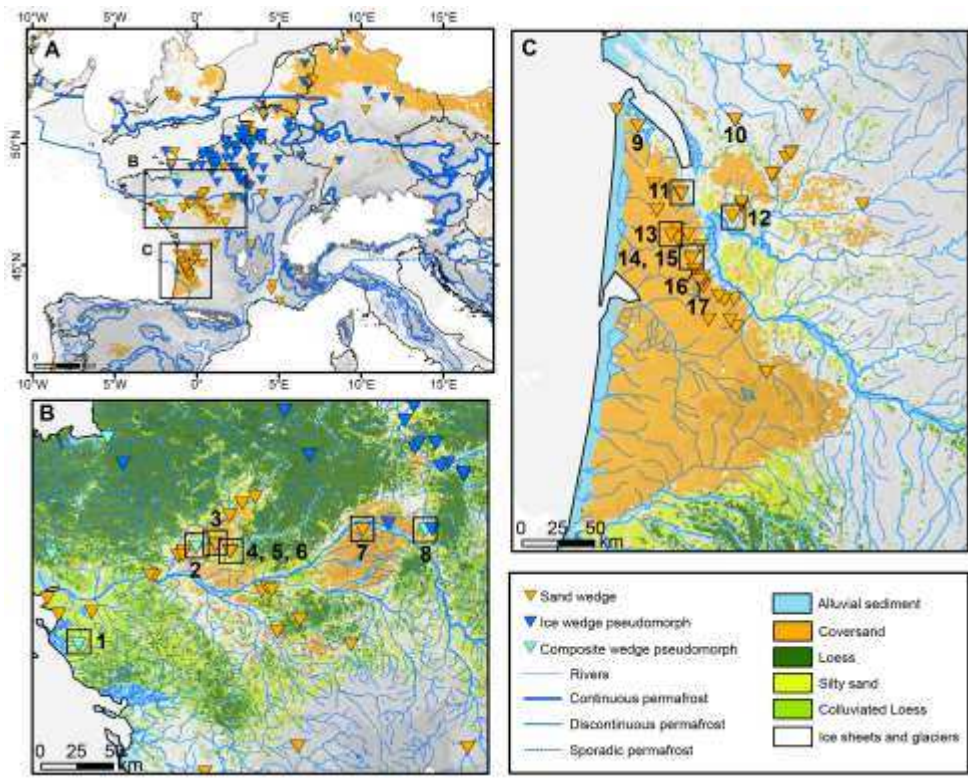
- 553 Lautridou, J.P., 1985. Le cycle périglaciaire pléistocène en Europe du nord-ouest et plus  
554 particulièrement en Normandie. Thèse d'Etat, Université de Caen, 487 pp.
- 555 Lécolle, F., 1989. Le cours moyen de la Seine au Pléistocène moyen et supérieur. Thèse, Caen et  
556 Université de Rouen, 549 pp.
- 557 Lenoble, A., Bertran, P., Mercier, N., Sitzia L., 2012. Le site du Lac Bleu et la question de l'extension du  
558 pergélisol en France au Pléistocène supérieur. Quaternaire continental d'Aquitaine : un point sur les  
559 travaux récents. Livret-guide de l'excursion AFEQ-ASF 2012, Université de Bordeaux, AFEQ, 107-121.
- 560 Locht, J. L., Antoine, P., Auguste, P., Bahain, J.J., Debehram, N., Falguères, C., Farkh, S., Tissoux, H.,  
561 2006. La séquence loessique Pléistocène supérieur de Savy (Aisne, France): stratigraphie, datations et  
562 occupations paléolithiques. Quaternaire, 17, 269–275.
- 563 Maarleveld, G.C., 1976. Periglacial phenomena and the mean annual air temperature during the last  
564 glacial time in The Netherlands. Biuletyn Periglacialny, 26, 57–78.
- 565 Mackay, J.R., 1993. Air temperature, snow cover, creep of frozen ground, and the time of ice-wedge  
566 cracking, western Arctic coast. Canadian Journal of Earth Sciences, 30 (8), 1720-1729.
- 567 Mejdhal, V., 1979. Thermoluminescence dating: Beta-dose attenuation in quartz grains.  
568 Archaeometry 21, 61-72.
- 569 Meszner, S., Kreutzer, S., Fuchs M., Faust, D., 2013. Late Pleistocene landscape dynamics in Saxony,  
570 Germany: Paleoenvironmental reconstruction using loess-paleosol sequences. Quaternary  
571 International, 296, 94-107.
- 572 Michel, J. P., 1969. Divers types de phénomènes périglaciaires et leur répartition dans les alluvions  
573 quaternaires de la Seine et de ses affluents. Supplément du Bulletin de l'Association Française pour  
574 l'Etude du Quaternaire 2, 721-735.
- 575 Michel, J.P., 1975. Périglaciaires des environs de Paris. Biuletyn Peryglacialny, 24, 259-352.
- 576 Moine, O., Antoine, P., Deschodt, L., Sellier-Segard, N., 2011. Enregistrements malacologiques à  
577 haute résolution dans les loess et les gleys de tundra du Pléniglaciaire weichsélien supérieur:  
578 premiers exemples du nord de la France. Quaternaire 22, 307-325.
- 579 Murray, A.S., Wintle, A.G., 2000. Luminescence dating of quartz using an improved single- aliquot  
580 regenerative-dose protocol. Radiation Measurements 32, 57-73.

- 581 Murray, A.S., Wintle, A.G., 2003. The single aliquot regenerative dose protocol: Potential for  
582 improvements in reliability. *Radiation Measurements*, 37, 377-381.
- 583 Murton, J.B., 2013. Permafrost and Periglacial Features. Ice Wedges and Ice-Wedge Casts. In  
584 *Encyclopedia of Quaternary Science (Second Edition)*, Elsevier, Amsterdam, 436-451.
- 585 Murton, J.B., Worsley, P., Gozdzik, J., 2000. Sand veins and wedges in cold Aeolian environments.  
586 *Quaternary Science Reviews*, 19 (9), 899-922.
- 587 Olley, J., Caitcheon, G., Murray, A., 1998. The distribution of apparent dose as determined by optical  
588 stimulated luminescence in small aliquots of fluvial quartz: Implications for dating young sediments.  
589 *Quaternary Geochronology*, 17, 1033-1040.
- 590 Péwé, T.L., 1966. Palaeoclimatic significance of fossil ice wedges. *Biuletyn Peryglacjalny*, 5, 65-72.
- 591 Ponel, P., Gandouin, E., Russell Coope, G., Andrieu-Ponel, V., Guiter, F., Van Vliet-Lanoë, B., Franquet,  
592 E., Brocandel, M., Brulhet, J., 2007. Insect evidence for environmental and climate changes from  
593 Younger Dryas to Sub-Boreal in a river floodplain at St-Momelin (St-Omer basin, northern France),  
594 Coleoptera and Trichoptera. *Palaeogeography, Palaeoclimatology, Palaeoecology* 245, 483-504.
- 595 Prescott, J.R., Hutton, J.T., 1994. Cosmic-ray contributions to dose-rates for luminescence and ESR  
596 dating – Large depths and long-term time variations. *Radiation Measurements* 23, 497-500.
- 597 Rasmussen, S. O., Bigler, M., Blockley, S. P., Blunier, T., Buchardt, S. L., Clausen, H. B., Cvijanovic, I.,  
598 Dahl-Jensen, D., Johnsen, S. J., Fischer, H., Gkinis, V., Guillevic, M., Hoek, W. Z., Lowe, J. J., Pedro, J.,  
599 Popp, T. J., Seierstad, I. K., Steffensen, J. P., Svensson, A., Vallelonga, P. T., Vinther, B. M., Walker, M.  
600 J. C., Wheatley, J. J., Winstrup, M., 2014. A stratigraphic framework for abrupt climatic changes during  
601 the Last Glacial period based on three synchronized Greenland ice-core records: refining and  
602 extending the INTIMATE event stratigraphy. *Quaternary Science Reviews*, 106, 14-28.
- 603 Readhead, M.L., 2002. Absorbed dose fraction for  $^{87}\text{Rb}$  beta particles. *Anc. TL* 20, 25-29.
- 604 Renssen, H., Isarin, R.F.B., 1998. Surface temperature in NW Europe during the Younger Dryas: AGCM  
605 simulation compared with climate reconstructions. *Climate Dynamics*, 14, 33-44.
- 606 Roberts, R.G., Galbraith, R.F., Yoshida, H., Laslett, G.M., Olley, J.M., 2000. Distinguishing dose  
607 populations in sediment mixtures: a test of optical dating procedures using mixtures of laboratory-  
608 dosed quartz. *Radiation Measurements*, 32, 459-465.

- 609 Sanchez-Goñi, M.F., Harrison S.P., 2010. Millennial-scale climate variability and vegetation changes  
610 during the LastGlacial: Concepts and terminology. *Quaternary Science Reviews* 29, 2823-2827.  
611
- 612 Sellier, N., Coutard, S., 2007. Données récentes sur le Paléolithique moyen de l'Aisne : une  
613 occupation du Weichselien ancien à Courmelles. *Revue archéologique de Picardie* 3-4, 5-16.
- 614 Sommé, J., Tuffreau., A., 1971. Stratigraphie du Pléistocène récent et Moustérien de Tradition  
615 Acheuléenne à Marcoing (Cambresis – nord de la France). *Bulletin de l'Association Française pour*  
616 *l'Etude du Quaternaire* 2, 57-74.
- 617 Simonis, D., Hense, A., Litt, T., 2012. Reconstruction of late Glacial and Early Holocene near surface  
618 temperature anomalies in Europe and their statistical interpretation. *Quaternary International*, 274,  
619 233-250.
- 620 Sitzia, L., Bertran, P., Bahain, J.J., Bateman, M.D., Hernandez, M., Garon, H., De Lafontaine, G.,  
621 Mercier, N., Leroyer, C., Queffelec A., Voinchet, P., 2015. The quaternary coversands of southwest  
622 France. *Quaternary Science Reviews*, 124, 84-105.
- 623 Tricart, J., 1956. Carte des phénomènes périglaciaires quaternaires en France. Mémoire pour servir à  
624 l'explication de la carte géologique détaillée de la France. Ministère de l'Industrie et du Commerce:  
625 Paris.
- 626 Vandenberghe, D., De Corte, F., Buylaert, J.-P., Kucera, J., Van Den Haute, P., 2008. On the internal  
627 radioactivity in quartz. *Radiation Measurements*, 43, 771-775.
- 628 Vandenberghe, J., 1983. Ice-wedge casts and involutions as permafrost indicators and their  
629 stratigraphic position in the Weichselian. *Proceedings of the 4th International Conference on*  
630 *Permafrost, Fairbanks, Alaska*, 1, 1298-1302.
- 631 Vandenberghe, J., Lowe, J., Coope, G. R., Litt, T., & Zöller, L., 2004. Climatic and environmental  
632 variability in the Mid-Latitude Europe sector during the last interglacial-glacial cycle. In R. Battarbee,  
633 F. Gasse, & C. Stickley (Eds.), *Past Climate Variability through Europe and Africa: PEPIII Conference*  
634 *Proceedings* (pp. 393-416). Dordrecht: Kluwer.
- 635 Vandenberghe, J., French, H., Gorbunov, A., Marchenko, S., Velichko, A.A., Jin, H., Cui, Z., Zhang, T.,  
636 Wan, X., 2014. The Last permafrost Maximum (LPM) map of the Northern Hemisphere: permafrost  
637 extent and mean annual air temperatures, 25-17 ka. *Boreas*, 43, 652-666.

- 638 Van Vliet-Lanoë, B., Hallégouët, B., 2001. European permafrost at the LGM and at its maximal extent.  
639 The geological approach. In *Permafrost Response on Economic Development, Environmental Security*  
640 *and Natural Resources*, Paepe R, Melnikov V (eds). Kluwer Academic Publishers: Dordrecht, 195–213.
- 641 Wanner, H., Solomina, O., Grosjean, M., Ritz, S.P., Markéta, J., 2011. Structure and origin of Holocene  
642 cold events. *Quaternary Science reviews*, 30, 3109-3123.
- 643 Williams, R.B.G., 1968. Periglacial climate and its relation to landforms: a study of southern and  
644 eastern England during the Last Glacial Period. PhD Thesis, University of Cambridge.
- 645 Wojdyr, M.J., 2010. Fityk: a general-purpose peak fitting program. *Journal of Applied Crystallography*  
646 43, 1126-1128.
- 647 Wolfe, S.A., Morse, P.D., Kokelj, S.V., Neudorf, C.M., Lian, O.B., 2016. Contrasting environments of  
648 sand wedge formation in discontinuous permafrost, Great Slave High Boreal Plains, Northwest  
649 Territories, Canada. Abstracts, 11<sup>th</sup> international conference on permafrost, 20-24 June 2016,  
650 Potsdam, Germany, 112.
- 651
- 652
- 653

654 Figures:

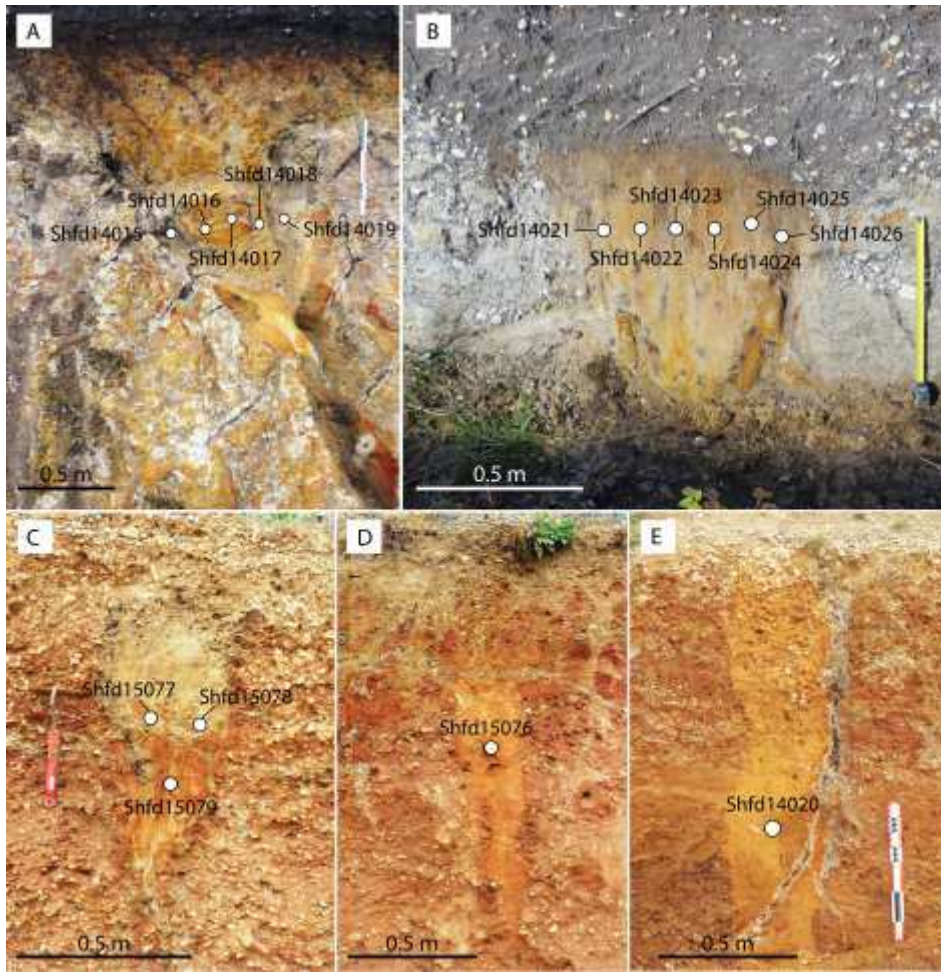


655

656 Figure 1: Spatial distribution of the relict periglacial wedge features in France and Northern Europe  
 657 with zooms on A) Loire valley and B) Northern Aquitaine. OSL dating was carried out on the  
 658 numbered features, the ones dated therein are highlighted with a black square. 1 Challans ; 2 Durtal ;  
 659 3 La Flèche ; 4, 5, 6 La-Chapelle-aux-Choux ; 7 Olivet ; 8 Sainte-Geneviève-des-Bois ; 9 Jau-Dignac ; 10  
 660 Jonzac (Guhl et al., 2013) ; 11 Cussac-Fort-Médoc ; 12 Saint-André-de-Cubzac ; 13 Salaunes ; 14, 15  
 661 Mérignac ; 16 Pessac Cap-de-Bos, 17 Léognan Lac Bleu (Lenoble et al., 2012). Northern Europe data  
 662 was extracted from Isarin et al. (1998) and France data from Andrieux et al. (2016a, 2016b). The  
 663 permafrost limits (thick, fine, and dotted lines) were drawn on figure 1A according to the modelled  
 664 LGM isotherms provided by K. Saito (Saito et al., 2013) that best fit with the mapped periglacial  
 665 features.

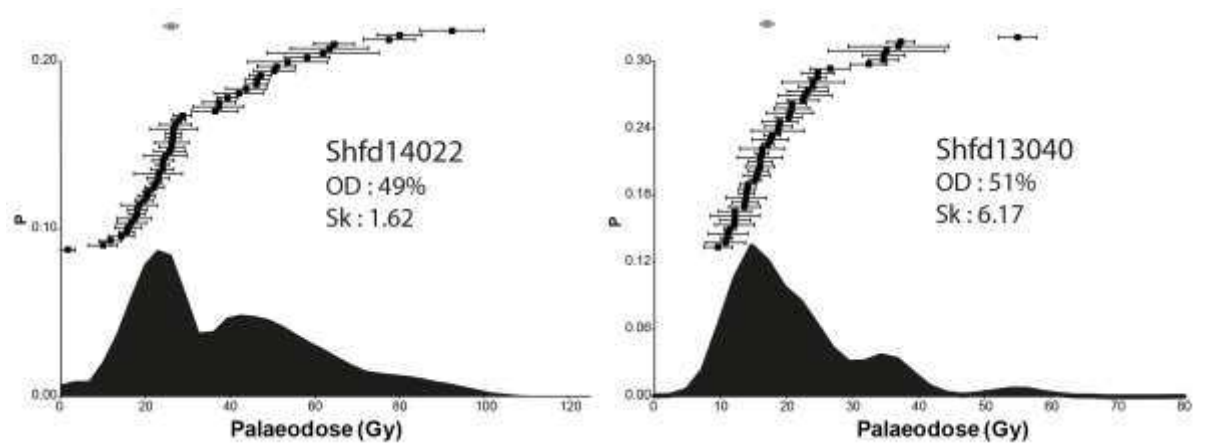
666





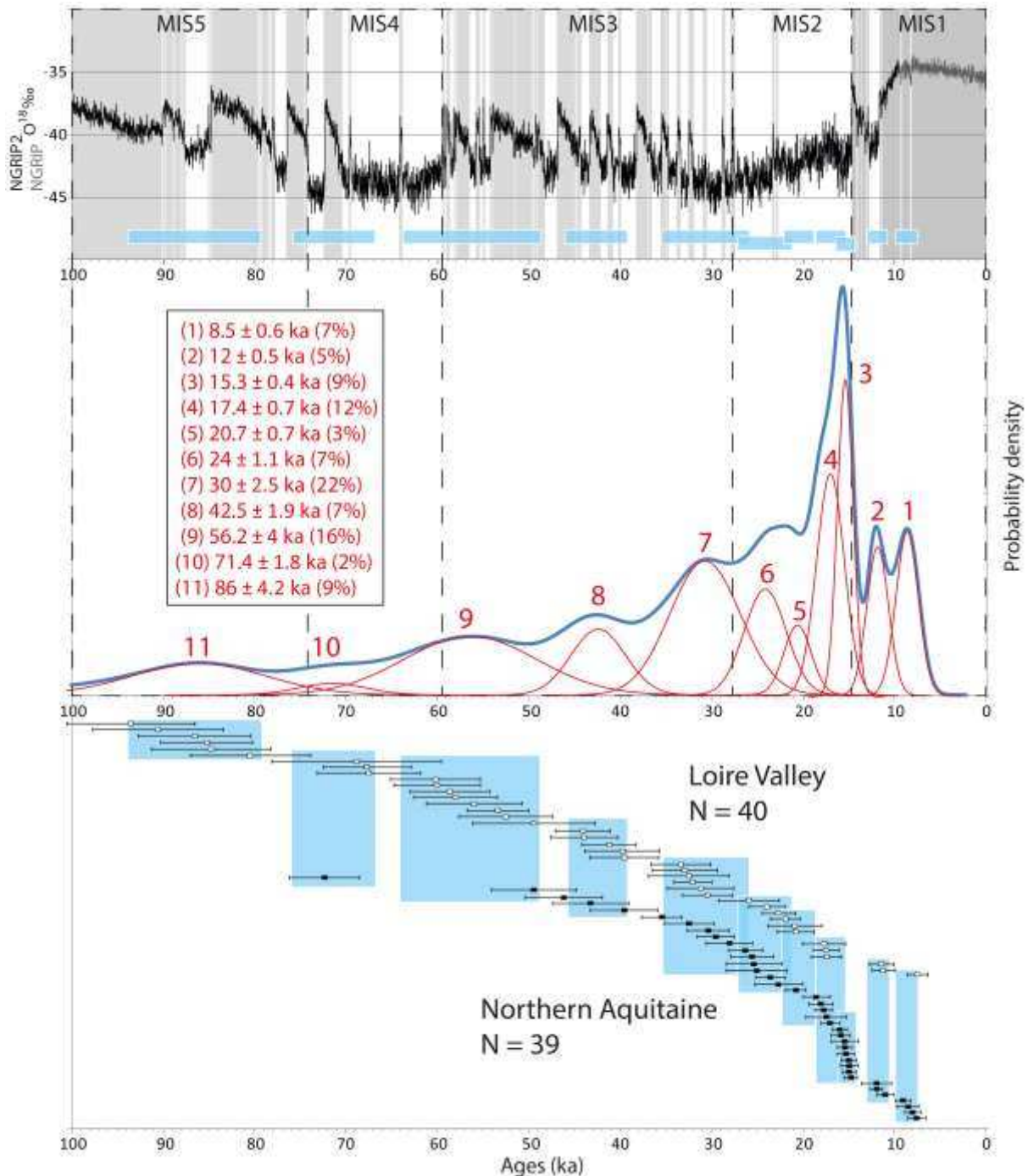
667

668 Figure 2: Relict sand-wedges in A) Méridnac (Chronopost), B) Cussac-Fort-Médoc (Parcelle Lagrange),  
 669 C) and D) La Chapelle-aux-Choux, E) Saint-Christophe-du-Lignerion (Challans)

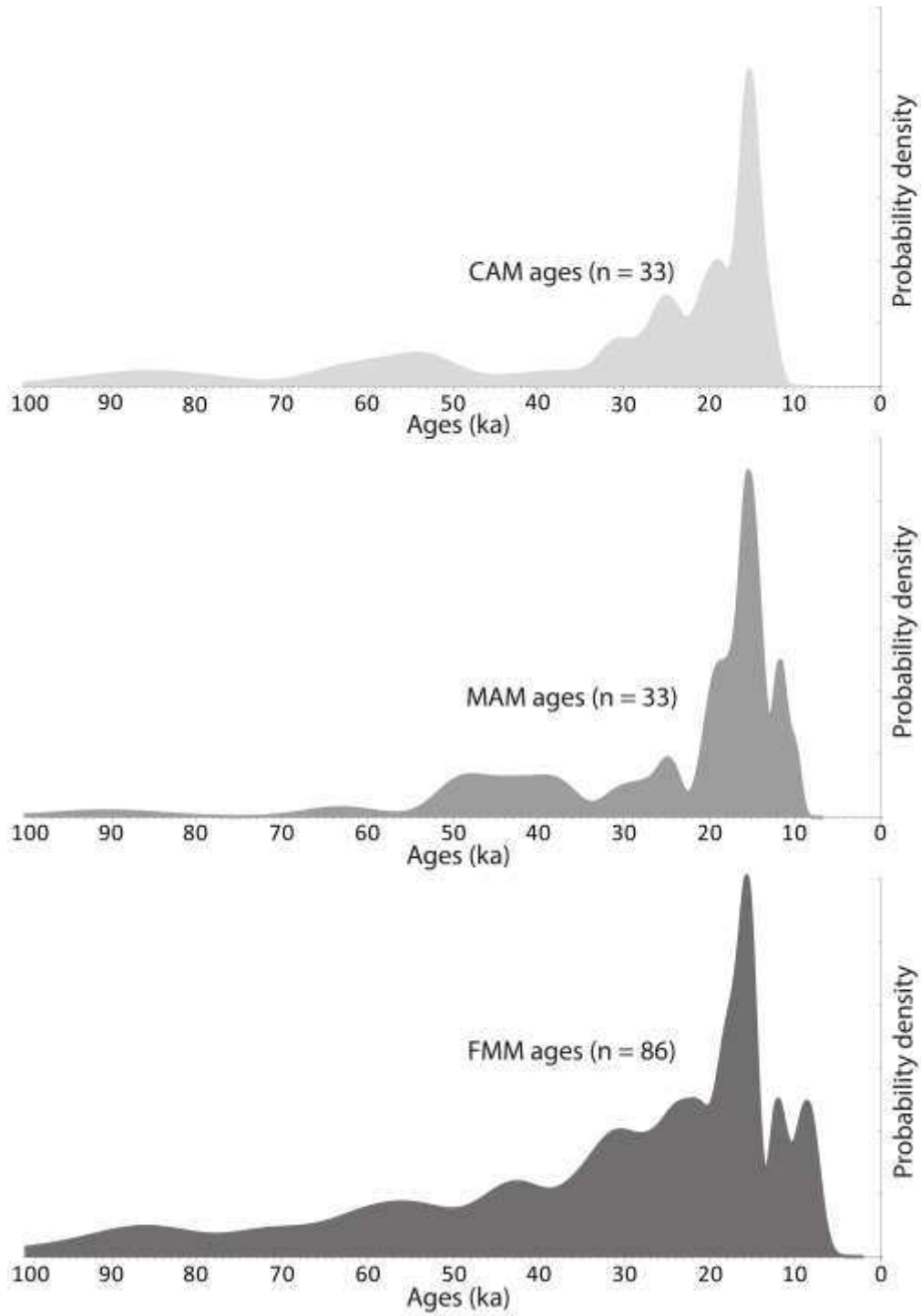


670

671 Figure 3: Examples of probability density functions (pdf) plotted for the single grain samples  
 672 Shfd13040 and Shfd14022 with the individual grain results above (Black) and mean (grey) showing  
 673 multiple De components. Overdispersion values (OD) were calculated as per Galbraith et al., (1999),  
 674 skewness (Sk) as per Bailey and Arnold (2006). N = number of measured grains.



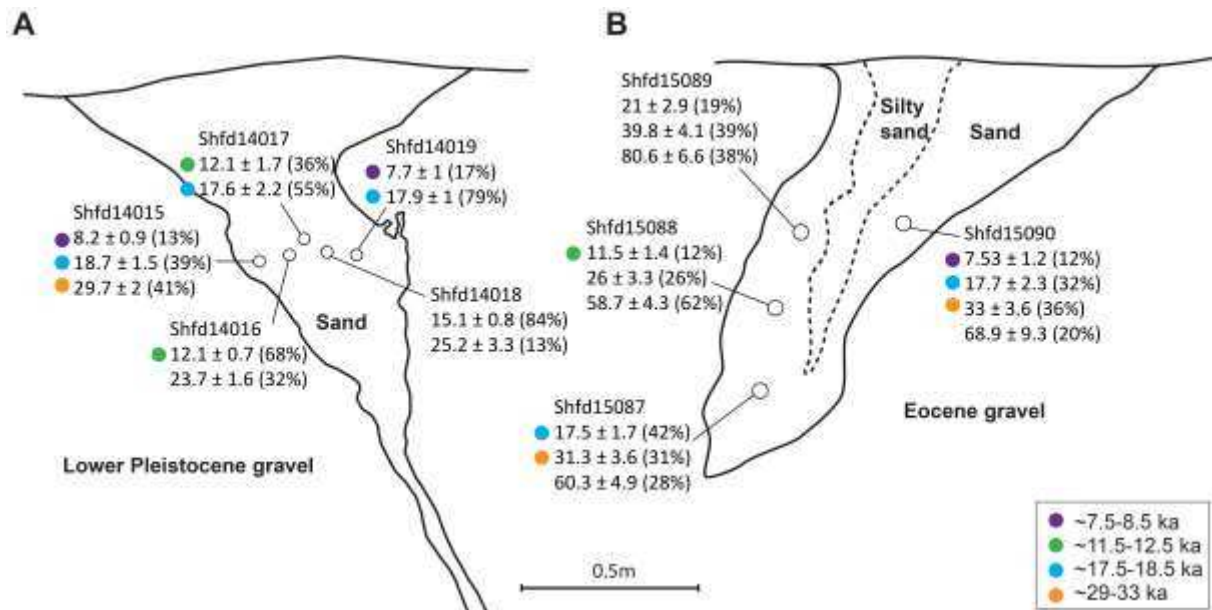
675  
 676 Figure 4: Probability density of the FMM ages (blue line) and FMM estimates of the Loire valley  
 677 (white) and Northern Aquitaine (black), plotted together with the NGRIP  $\delta^{18}\text{O}$  data over the last 100  
 678 ka tuned to the revised Greenland Ice Core Chronology proposed by Rasmussen et al. (2014). The  
 679 distribution of the probability density function was adjusted to a combination of Gaussian functions  
 680 (red lines) using the software Fityk 0.9.8 (Wojdyr, 2010). The respective contribution of each  
 681 Gaussian function to the dataset was expressed as a percentage of the total. The goodness of fit was  
 682 assessed using  $R^2$ , which reached almost unity ( $R^2=0.9999$ ). Blue boxes in the NGRIP curve and over  
 683 the age estimates represent the Full Width at Half Maximum (FWHM) of each Gaussian function  
 684 fitted. Grey shading represent the interglacial and greenland interstadials.



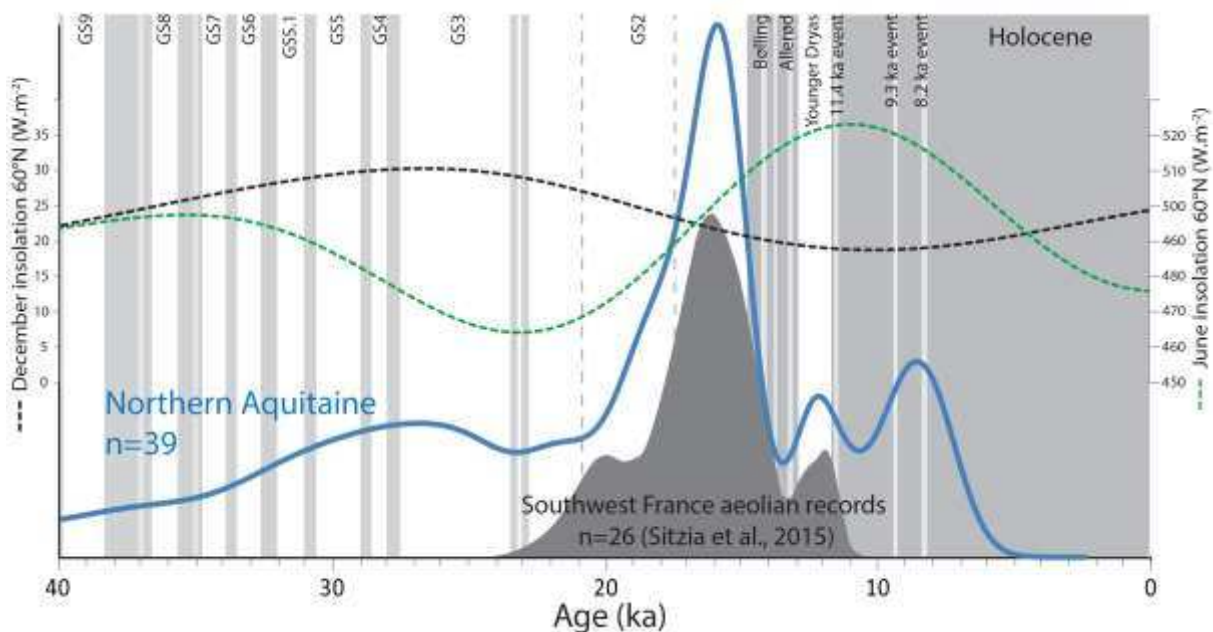
685

686

Figure 5: Probability density function of the ages calculated with A) CAM, B) MAM, and C) FMM.



687  
 688 Figure 6: Representative case study of two wedges sampled A) Mérignac (Chronopost) and B) Sainte-  
 689 Genevieve-des-bois (Les Bézards). OSL ages are calculated from FMM components which  
 690 contribution in the sample is shown in percentage. Coloured circles show the overlap of ages  
 691 between the samples and their belonging to an age cluster.



692  
 693 Figure 7 : Probability density of the sand wedge ages in Northern Aquitaine compared with the  
 694 aeolian records from southwest France (Sitzia et al., 2015) and the insolation in June and December  
 695 at 60°N (Berger, 1978). Interstadials and the Holocene are illustrated by grey shading and light grey  
 696 indicates cold sub-events (Rasmussen et al., 2014).

697

698

699 Table 1: Location of the studied features

<b>Area</b>	<b>Site</b>	<b>Lab code</b>	<b>Latitude (° WGS84)</b>	<b>Longitude (° WGS84)</b>	<b>Altitude (m a.s.l.)</b>
Northern Aquitaine	Salaunes (Château- Montgaillard)	Shfd142011, Shfd14012, Shfd14013, Shfd14014	44.935	-0.821	49
	Mérignac (Chronopost)	Shfd14015, Shfd14016, Shfd14017, Shfd14018, Shfd14019, Shfd12099	44.827	-0.689	47
	Cussac-Fort-Médoc (Parcelle Lagrange)	Shfd14021, Shfd14022, Shfd14023, Shfd14024, Shfd14025	45.114	-0.75	38
	Saint-André-de-Cubzac (ZAC Parc d'Aquitaine)	Shfd12098	45.01	0.26	52
	Olivet	Shfd15085, Shfd15086	47.815	1.927	114
Loire valley	Sainte-Geneviève-des-Bois (Les Bézards)	Shfd15087, Shfd15088, Shfd15089, Shfd15090	47.81	2.742	145
	La-Chapelle-aux-Choux	Shfd15077, Shfd15078, Shfd15079, Shfd15083, Shfd15084	47.617	0.211	69
	Durtal (Les Rairies)	Shfd13040, Shfd14028	47.66	-0.231	39
	Challans (Saint-Christophe-du- Ligneron)	Shfd14020	46.8	1.76	32
	La Flèche (La Louverie)	Shfd14027	47.685	-0.01	34

700

701 Table 2: Elemental and associated data used to calculate OSL sample dose rates.

Site	Sample	Lab code	K (%)	U (ppm)	Th (ppm)	Rb (ppm)	Alpha (uGy/ka)	Beta (uGy/ka)	Gamma (uGy/ka)	Mean Overburden (m)	Cosmic (uGy/ka)	Water content (%)	Dose rate (μGy/a)
Salaunes - Château Montgaillard	Montg13.1	Shfd14011	0.4 ± 0.02	0.87 ± 0.087	3.7 ± 0.37	26 ± 2.6	22 ± 4	589 ± 40	337 ± 22	1.1	182 ± 9	8.7 ± 5	1130 ± 46
	Montg13.2	Shfd14012	0.4 ± 0.02	0.67 ± 0.067	3 ± 0.3	21.8 ± 2.18	20 ± 4	563 ± 39	304 ± 20	1.1	182 ± 9	3.8 ± 5	1070 ± 44
	Montg13.3	Shfd14013	0.4 ± 0.02	0.67 ± 0.067	3 ± 0.3	19.9 ± 1.99	20 ± 3	552 ± 38	305 ± 20	1	184 ± 9	3.7 ± 5	1062 ± 44
	Montg13.4	Shfd14014	0.4 ± 0.02	0.63 ± 0.063	2.8 ± 0.28	21.1 ± 2.11	19 ± 2	535 ± 37	283 ± 18	0.85	188 ± 9	6 ± 5	1026 ± 42
Cussac-Fort Médoc - Parcelle Lagrange	Cu13.1	Shfd14021	0.4 ± 0.02	0.61 ± 0.061	2 ± 0.2	19 ± 1.9	18 ± 4	531 ± 37	258 ± 17	0.61	193 ± 10	1.8 ± 5	1001 ± 42
	Cu13.2	Shfd14022	0.5 ± 0.025	1.73 ± 0.173	4.2 ± 0.42	27.1 ± 2.71	28 ± 3	802 ± 55	487 ± 31	0.61	193 ± 10	5.5 ± 5	1510 ± 48
	Cu13.3	Shfd14023	0.4 ± 0.02	0.59 ± 0.059	2 ± 0.2	16.6 ± 1.66	18 ± 3	516 ± 37	257 ± 16	0.61	193 ± 10	1.4 ± 5	984 ± 32
	Cu13.4	Shfd14024	0.4 ± 0.02	0.72 ± 0.072	1.9 ± 0.19	16.2 ± 1.62	18 ± 3	520 ± 37	263 ± 17	0.61	193 ± 10	2.5 ± 5	995 ± 41
	Cu13.5	Shfd14025	0.5 ± 0.025	0.61 ± 0.061	2.4 ± 0.24	20.4 ± 2.04	19 ± 4	623 ± 44	302 ± 19	0.61	193 ± 10	1.6 ± 5	1138 ± 49
	Cu13.6	Shfd14026	0.6 ± 0.03	0.75 ± 0.075	2.9 ± 0.29	29.7 ± 2.97	21 ± 4	770 ± 54	359 ± 23	0.61	193 ± 10	3 ± 5	1343 ± 59
Mérignac - Chronopost	MC13.1	Shfd14015	0.4 ± 0.02	0.99 ± 0.099	4.2 ± 0.42	22.3 ± 2.23	22 ± 2	501 ± 34	318 ± 20	0.9	187 ± 9	20.4 ± 5	1221 ± 50
	MC13.2	Shfd14016	0.5 ± 0.03	1.04 ± 0.104	5.2 ± 0.52	27.7 ± 2.77	24 ± 4	623 ± 42	389 ± 25	0.9	187 ± 9	18.5 ± 5	1357 ± 56
	MC13.3	Shfd14017	0.4 ± 0.02	0.88 ± 0.088	4.3 ± 0.43	24.6 ± 2.46	22 ± 3	552 ± 37	340 ± 22	0.9	187 ± 9	14.1 ± 5	1189 ± 48
	MC13.4	Shfd14018	0.4 ± 0.02	0.71 ± 0.071	3.1 ± 0.31	20.7 ± 2.07	19 ± 4	455 ± 31	257 ± 16	0.9	187 ± 9	19.3 ± 5	1060 ± 43
	MC13.5	Shfd14019	0.4 ± 0.02	0.85 ± 0.085	3.7 ± 0.37	22.3 ± 2.23	20 ± 2	474 ± 32	284 ± 18	0.9	187 ± 9	21.2 ± 5	1139 ± 46
	Chronopost 1	Shfd12099	0.3 ± 0.02	0.88 ± 0.088	3.4 ± 0.34	24.1 ± 2.41	23 ± 2	567 ± 51	336 ± 22	2	161 ± 8	5.2 ± 5	1029 ± 42
Saint André de Cubzac	St André 2	Shfd12098	1.2 ± 0.06	0.95 ± 0.095	3.8 ± 0.38	53.8 ± 5.38	23 ± 2	1311 ± 95	535 ± 34	1.8	165 ± 8	7.8 ± 5	2034 ± 102
La Chapelle aux Choux	CAH1.1	Shfd15076	0.4 ± 0.02	0.87 ± 0.087	4.4 ± 0.44	27.8 ± 2.78	24 ± 2	639 ± 43	382 ± 25	1.2	180 ± 9	5.6 ± 5	1225 ± 50

	CAH2.1	Shfd15077	0.5 ± 0.03	1.42 ± 0.142	7.1 ± 0.71	46.1 ± 4.61	30 ± 2	825 ± 55	518 ± 33	0.6	196 ± 10	15.16 ± 5	1569 ± 66
	CAH2.2	Shfd15078	0.4 ± 0.02	1.1 ± 0.11	5.6 ± 0.56	40.5 ± 4.05	26 ± 2	702 ± 47	423 ± 27	0.6	196 ± 10	12.29 ± 5	1347 ± 56
	CAH2.3	Shfd15079	0.4 ± 0.02	0.99 ± 0.099	5.7 ± 0.57	46.1 ± 4.61	26 ± 2	740 ± 50	426 ± 28	0.8	190 ± 10	10.62 ± 5	1382 ± 58
	CAH4.1	Shfd15083	0.2 ± 0.01	0.56 ± 0.056	2 ± 0.2	7.2 ± 0.72	18 ± 3	303 ± 22	203 ± 13	0.6	196 ± 10	2 ± 5	720 ± 27
	CAH4.2	Shfd15084	0.2 ± 0.01	0.44 ± 0.044	1.5 ± 0.15	6.6 ± 0.66	16 ± 2	272 ± 19	166 ± 11	0.9	188 ± 9	2.5 ± 5	642 ± 24
Olivet	O1	Shfd15085	2.5 ± 0.13	1.25 ± 0.125	4.5 ± 0.45	110 ± 11	27 ± 2	2789 ± 211	962 ± 64	1	187 ± 9	1.4 ± 5	3689 ± 202
	O2	Shfd15086	2.7 ± 0.14	1.64 ± 0.164	6.5 ± 0.65	126 ± 12.6	33 ± 2	2969 ± 218	1094 ± 72	1.4	177 ± 9	5.5 ± 5	4483 ± 241
Saint Geneviève des Bois - Les Bézards	B1	Shfd15087	2.4 ± 0.12	1.38 ± 0.138	7.7 ± 0.77	119 ± 11.9	34 ± 2	2713 ± 197	1051 ± 68	1.5	175 ± 9	5.5 ± 5	3973 ± 209
	B2	Shfd15088	2.2 ± 0.11	1.36 ± 0.136	7.1 ± 0.71	110 ± 11	31 ± 2	2343 ± 171	917 ± 59	1.2	183 ± 9	10.5 ± 5	3695 ± 193
	B3	Shfd15089	1.2 ± 0.06	1.47 ± 0.147	8.1 ± 0.81	77.7 ± 7.77	35 ± 2	1589 ± 109	772 ± 49	1	188 ± 9	8.2 ± 5	2583 ± 121
	B4	Shfd15090	2.5 ± 0.13	1.31 ± 0.131	7 ± 0.7	121 ± 12.1	32 ± 2	2779 ± 204	1038 ± 68	1	188 ± 9	5.3 ± 5	4037 ± 215
Durtal	Durtal	Shfd14028	0.3 ± 0.02	0.5 ± 0.05	2.3 ± 0.23	14.7 ± 1.47	18 ± 3	320 ± 25	228 ± 15	0.8	189 ± 9	3.9 ± 5	755 ± 30
	Durtal 3	Shfd13040	0.2 ± 0.01	0.45 ± 0.045	1.6 ± 0.16	14.1 ± 1.41	16 ± 2	310 ± 22	165 ± 11	1.1	181 ± 9	5.6 ± 5	673 ± 25
Challans	Challans 2	Shfd14020	0.8 ± 0.04	1.24 ± 0.124	5.3 ± 0.53	43.4 ± 4.34	28 ± 2	1051 ± 73	543 ± 35	1.1	181 ± 9	7.2 ± 5	1803 ± 81
La Louverie	Lou3	Shfd14027	0.2 ± 0.01	0.42 ± 0.042	1.8 ± 0.18	11.7 ± 1.17	16 ± 3	236 ± 19	178 ± 11	0.6	194 ± 10	1.6 ± 5	626 ± 24

703

704 Table 3: Finite Model Mixture (FMM) ages in comparison with the estimates calculated from the Central Age Model (CAM) and Minimum Age Model (MAM)

Site	Sample	Lab code	CAM		FMM		
			De (Gy)	Age (ka)	De Component (Gy)	De Component (%)	Age (ka)
Salaunes - Château Montgaillard	Montg13.1	Shfd14011	27.11 ± 1.56	23.98 ± 1.69	17.5161 ± 1.513	25	15.58 ± 1.49
					29.9071 ± 1.708	57	26.46 ± 1.86
					52.324 ± 4.285	17	46.29 ± 4.24
	Montg13.2	Shfd14012	16.19 ± 0.92	15.13 ± 1.06	16.6355 ± 0.541	74	15.55 ± 0.82
					34.8896 ± 2.547	18	32.61 ± 2.74
	Montg13.3	Shfd14013	16.68 ± 0.85	15.71 ± 1.03	16.401 ± 0.709	72	15.45 ± 0.92
					27.092 ± 3.021	17	25.52 ± 3.03
	Montg13.4	Shfd14014	20.88 ± 0.92	20.36 ± 1.23	8.872 ± 1.189	10	8.65 ± 1.21
					21.4495 ± 0.719	76	20.91 ± 1.11
	Cussac-Fort Médoc - Parcelle Lagrange	Cu13.1	Shfd14021	56.09 ± 3.51	56.05 ± 4.22	40.6771 ± 3.384	14
30.5052 ± 1.968						27	30.49 ± 2.35
Cu13.2		Shfd14022	27.87 ± 1.88	18.45 ± 1.37	72.4853 ± 2.392	73	72.44 ± 3.87
					22.51 ± 0.887	63	14.9 ± 0.75
Cu13.3		Shfd14023	15.5 ± 0.7	15.75 ± 0.97	53.684 ± 2.443	37	35.55 ± 2.21
					14.8822 ± 0.588	80	15.12 ± 0.77
Cu13.4		Shfd14024	15.81 ± 0.98	15.89 ± 1.19	22.4762 ± 2.434	18	22.83 ± 2.65
					15.0239 ± 0.793	62	15.1 ± 1.02
Cu13.5		Shfd14025	17.37 ± 0.91	15.27 ± 1.04	25.5927 ± 2.111	30	25.72 ± 2.38
					18.3634 ± 0.562	73	16.14 ± 0.86
Cu13.6	Shfd14026	26.01 ± 2.38	19.36 ± 1.97	56.3969 ± 4.67	11	49.58 ± 4.64	
				15.0251 ± 1.127	25	11.18 ± 0.97	
Mérignac - Chronopost	MC13.1	Shfd14015	20.83 ± 1.38	20.27 ± 1.57	24.4409 ± 1.347	37	18.19 ± 1.29
					58.2539 ± 4.905	16	43.36 ± 4.13
	MC13.2	Shfd14016	17.3 ± 0.93	13.93 ± 0.95	156.2825 ± 13.925	22	116.33 ± 10.91
					8.4222 ± 0.824	13	8.18 ± 0.87
	MC13.3	Shfd14017	16.41 ± 0.77	14.9 ± 0.92	19.2245 ± 1.321	39	18.71 ± 1.48
					30.4879 ± 1.747	41	29.67 ± 2.07
	MC13.4	Shfd14018	14.07 ± 0.68	15.33 ± 0.96	14.7663 ± 0.534	68	12.08 ± 0.66
					29.001 ± 1.529	32	23.72 ± 1.58
	MC13.5	Shfd14019	14.92 ± 0.96	15.46 ± 1.17	13.3105 ± 1.762	36	12.09 ± 1.67
					19.3465 ± 2.3	55	17.57 ± 2.21
Chronopost 1	Shfd12099	18.98 ± 0.75	18.44 ± 1.05	13.8868 ± 0.507	84	15.13 ± 0.82	
				23.1301 ± 2.8843	13	25.2 ± 3.3	
				7.4434 ± 0.913	17	7.71 ± 0.99	
				17.2444 ± 0.607	79	17.87 ± 0.95	
				17.6972 ± 0.676	65	17.19 ± 0.97	

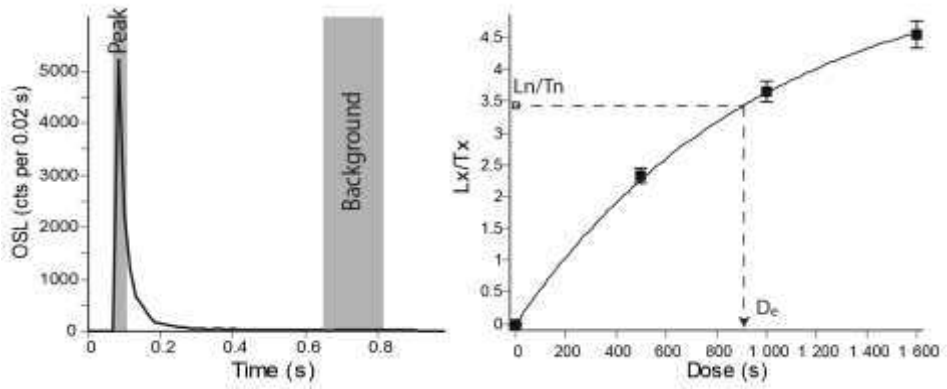


Saint André de Cubzac - ZAC parc d'Aquitaine	St André 2	Shfd12098	25.91 ± 1.17	12.74 ± 0.86	28.9987 ± 2.329	22	28.17 ± 2.54	
					18.7443 ± 1.336	31	9.21 ± 0.81	
	CAH1.1	Shfd15076	63.54 ± 3.03	51.86 ± 3.27	32.5813 ± 1.287	66	16.02 ± 1.02	
					54.0867 ± 2.921	46	44.14 ± 3.01	
					83.078 ± 4.81	45	67.8 ± 4.82	
					47.8942 ± 3.7692	21	30.53 ± 2.73	
CAH2.1	Shfd15077	94.8 ± 5.7	60.42 ± 4.42	94.3216 ± 6.244	46	60.12 ± 4.71		
				176.7245 ± 11.027	33	112.64 ± 8.46		
CAH2.2	Shfd15078	122.91 ± 8.11	91.22 ± 7.1	91.0753 ± 6.639	36	67.59 ± 5.66		
				180.2477 ± 8.2192	53	133.78 ± 8.22		
La Chapelle aux Choux	CAH2.3	Shfd15079	113.09 ± 9.12	81.8 ± 7.44	60.8352 ± 4.417	21	44 ± 3.69	
					125.3123 ± 8.421	43	90.64 ± 7.18	
	CAH4.1	Shfd15083	99.22 ± 8.19	137.81 ± 12.5	220.7999 ± 13.182	31	159.71 ± 11.66	
					67.4209 ± 4.355	29	93.64 ± 7.01	
					116.2007 ± 10.528	34	161.39 ± 15.84	
					228.8668 ± 18.035	28	317.88 ± 27.76	
CAH4.2	Shfd15084	53.62 ± 3.79	83.57 ± 6.7	25.4295 ± 2.2454	14	39.64 ± 3.81		
				54.726 ± 2.501	49	85.3 ± 5.05		
Olivet	O1	Shfd15085	118.83 ± 8	29.97 ± 2.6	113.4103 ± 10.037	24	176.77 ± 17.01	
					216.1 ± 24.657	10	336.82 ± 40.48	
	O2	Shfd15086	112.92 ± 7.6	26.43 ± 2.28	69.5658 ± 4.153	27	17.55 ± 1.43	
					132.4353 ± 10.833	41	33.4 ± 3.29	
	B1	Shfd15087	103.4 ± 7.86	26.03 ± 2.41	208.6423 ± 16.942	32	52.62 ± 5.16	
					48.236 ± 4.703	12	11.29 ± 1.26	
	B2	Shfd15088	125.09 ± 11.83	36.01 ± 3.89	97.257 ± 5.68	40	22.76 ± 1.81	
					176.3477 ± 8.288	47	41.27 ± 2.95	
	Saint Geneviève des Bois - Les Bézards	B3	Shfd15089	109.71 ± 10.71	42.47 ± 4.6	69.475 ± 5.44	42	17.49 ± 1.66
						124.2104 ± 13.806	31	31.26 ± 3.62
B4		Shfd15090	90.88 ± 10.09	22.51 ± 2.77	239.435 ± 15.016	28	60.27 ± 4.93	
					39.7643 ± 4.2667	12	11.45 ± 1.37	
Durtal		Shfd14028	40.82 ± 2.39	54.06 ± 3.84	90.2591 ± 10.569	26	25.98 ± 3.33	
					203.9413 ± 10.707	62	58.71 ± 4.34	
Durtal 3	Shfd13040	16.92 ± 0.74	25.15 ± 1.45	54.2115 ± 7.1722	19	20.98 ± 2.94		
				102.8782 ± 9.382	39	39.82 ± 4.08		
Durtal	Shfd13040	16.92 ± 0.74	25.15 ± 1.45	208.1408 ± 12.988	38	80.57 ± 6.58		
				30.3856 ± 4.376	12	7.53 ± 1.16		
Durtal	Shfd13040	16.92 ± 0.74	25.15 ± 1.45	71.5037 ± 8.623	32	17.71 ± 2.34		
				133.2005 ± 12.547	36	33 ± 3.57		
Durtal	Shfd13040	16.92 ± 0.74	25.15 ± 1.45	278.2291 ± 34.389	20	68.92 ± 9.28		
				18.1332 ± 1.3274	14	24.01 ± 2		
Durtal	Shfd13040	16.92 ± 0.74	25.15 ± 1.45	40.3646 ± 1.954	51	53.45 ± 3.36		
				64.0464 ± 4.221	32	84.81 ± 6.54		
Durtal	Shfd13040	16.92 ± 0.74	25.15 ± 1.45	14.7938 ± 0.928	56	21.99 ± 1.62		
				21.9162 ± 2.834	27	32.57 ± 4.39		

					37.7118 ± 3.2319	13	56.05 ± 5.25
					57.9666 ± 2.73	79	32.14 ± 2.1
Challans	Challans 2	Shfd14020	56.05 ± 2.01	31.08 ± 1.78	89.328 ± 11.371	12	49.53 ± 6.68
					13.0501 ± 1.163	14	20.86 ± 2.03
La Flèche	Lou3	Shfd14027	39.86 ± 2.02	63.71 ± 4.06	36.3304 ± 2.478	45	58.07 ± 4.55
					54.1907 ± 3.251	42	86.62 ± 6.18

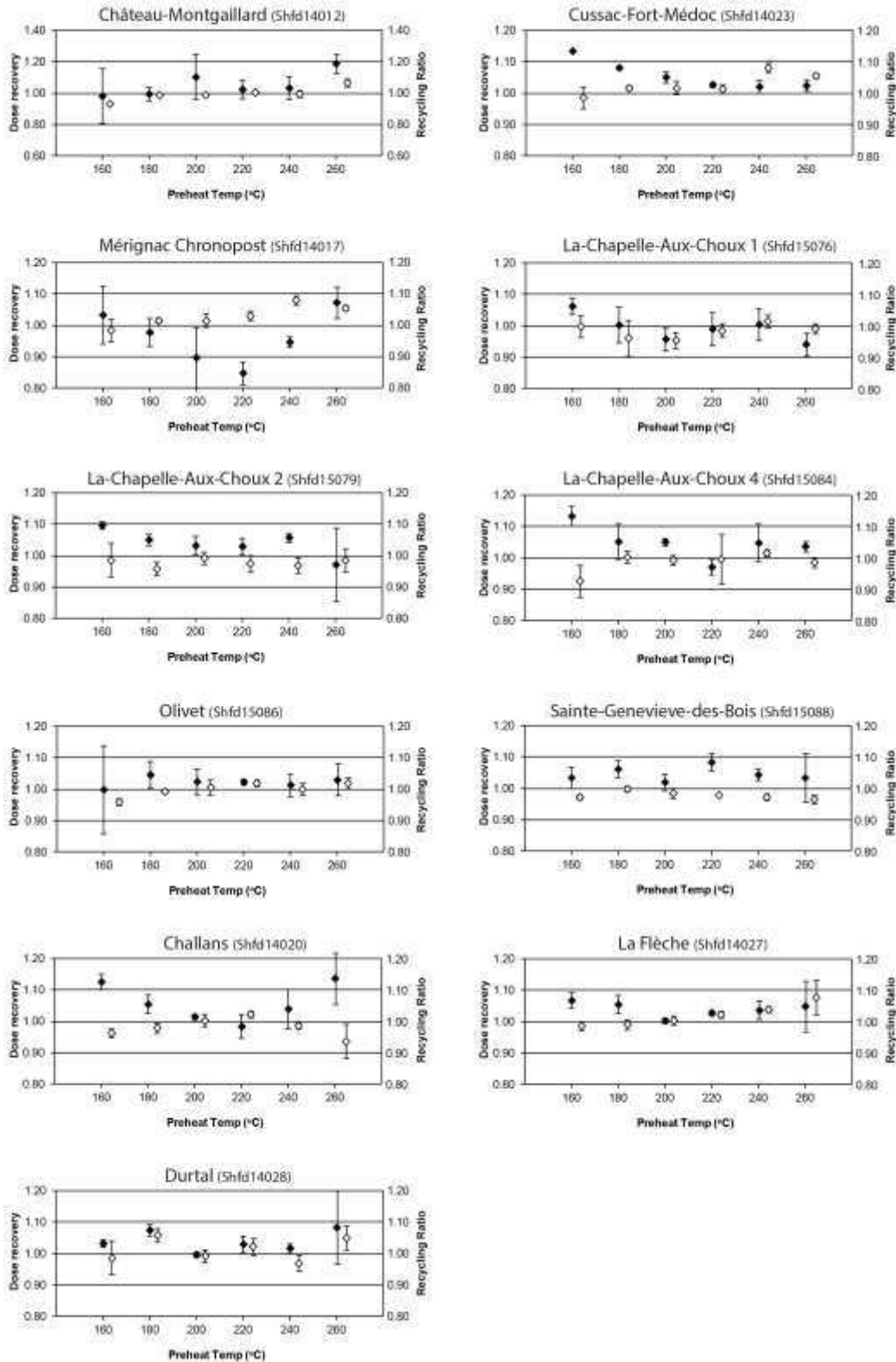
---

706



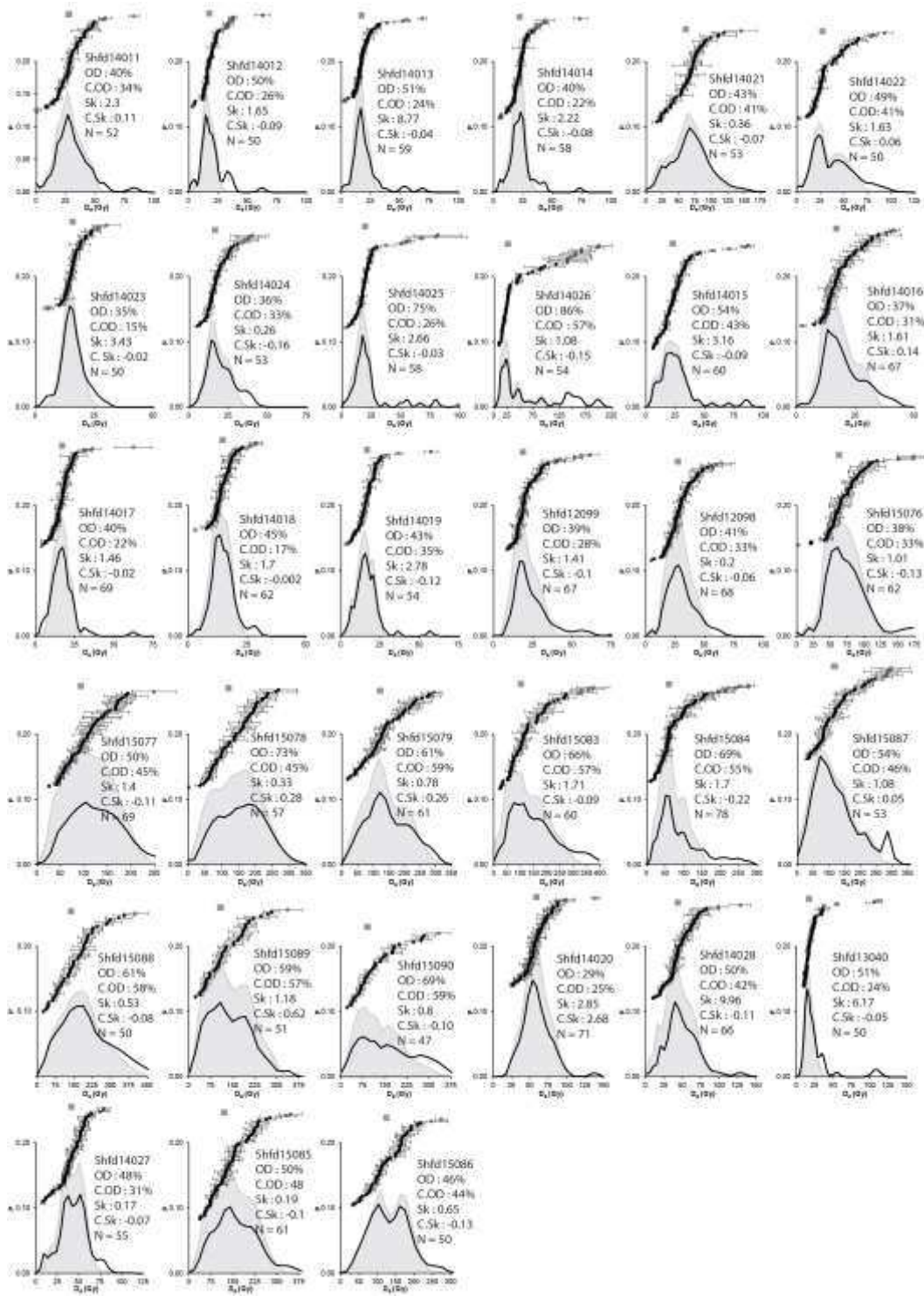
707

708 Figure A1: Single-aliquot regenerative dose (SAR) OSL decay curves and dose response curves for a  
709 single grain of sample Shfd14022. The used signal and background intervals are highlighted in grey.



710

711 Figure A2: Dose-recovery preheat plateau test performed on three small aliquots at each  
 712 temperature. The average values of the dose recovery (black) and the recycling ratio (white) are  
 713 presented with standard deviation. The solid line indicates the ideal values.



714

715 Figure A3: Probability density functions (pdf, solid line) plotted for all samples with the individual  
 716 grain results above (Black) and mean (dark grey), compared with the pdf (grey filled curve) of the same  
 717 data without outliers. Overdispersion values (OD), and OD without outliers (C.OD) were calculated as  
 718 per Galbraith et al., (1999), skewness (Sk) and Sk without outliers (C.Sk) as per Bailey and Arnold  
 719 (2006). N = number of measured grains.

720